This is a pre print version of the following article:

Isotopic constraints on contamination processes in the Tonian Goiás Stratiform Complex / Giovanardi, Tommaso; Mazzucchelli, Maurizio; Lugli, Federico; Girardi, Vicente A. V.; Correia, Ciro T.; Tassinari, Colombo C. G.; Cipriani, Anna. - In: LITHOS. - ISSN 0024-4937. - 310-311:(2018), pp. 136-152. [10.1016/j.lithos.2018.04.008]

Terms of use:

The terms and conditions for the reuse of this version of the manuscript are specified in the publishing policy. For all terms of use and more information see the publisher's website.

03/09/2024 07:41

(Article begins on next page)

Elsevier Editorial System(tm) for Lithos
Manuscript Draft

Manuscript Number: LITHOS6602

Title: The Tonian Goias Stratiform Complex: Lu-Hf isotopes evidences of crustal MORB contamination in mantle-derived melts

Article Type: Regular Article

Keywords: layered complex; contamination; Lu-Hf; zircon; Goias

Corresponding Author: Professor Maurizio Mazzucchelli, Full Professor

Corresponding Author's Institution: Università di Modena e Reggio Emilia

First Author: Tommaso Giovanardi

Order of Authors: Tommaso Giovanardi; Maurizio Mazzucchelli, Full Professor; Federico Lugli; Vicente Girardi, Full Professor; Ciro Correia, Professor; Colombo Tassinari, Full Professor; Anna Cipriani, Professor

Abstract: The Cana Brava, Niquelândia and Barro Alto complexes (Goiás, central Brazil) are three of the largest mafic-ultramafic layered complexes in the world. Recent geochemical, geochronological and structural evidences have constrained their origin from a single intrusion (i.e. the Tonian Goias Stratiform Complex), however, still debated is the style and source of contamination of the two sequences that characterize the complex. New in situ Lu-Hf zircon data suggest a strong crustal contamination of the Lower Sequence, but coherent with literature bulk-rock Rb-Sr and Sm-Nd systematics in Cana Brava and Niquelandia. The extremely low Hf isotope ratios are consistent with contamination from meta-pelitic and calc-silicate rocks found as xenoliths within the LS. The Upper Sequence zircons are characterized by more primitive Hf isotope ratios than the LS and in the scientific community have been largely considered uncontaminated. Our geochemical evaluation and modelling suggests that the US zircons have been affected by contamination from mantle-derived melts, which was masked in the Rb-Sr and Sm-Nd systematics, but in agreement with amphibolite xenoliths presence in the US stratigraphy. The Hf isotope composition of inherited zircons in both LS and US supports this hypothesis, showing negative εHf(t) values in inherited zircons from the LS and positive, mantle-derived εHf(t) values in inherited zircons from the US.

Abstract
Click here to download Abstract: Abstract_Lithos.docx

The Cana Brava, Niquelândia and Barro Alto complexes (Goiás, central Brazil) are three of the largest mafic-ultramafic layered complexes in the world. Recent geochemical, geochronological and structural evidences have constrained their origin from a single intrusion (i.e. the Tonian Goias Stratiform Complex), however, still debated is the style and source of contamination of the two sequences that characterize the complex. New in situ Lu-Hf zircon data suggest a strong crustal contamination of the Lower Sequence, but coherent with literature bulk-rock Rb-Sr and Sm-Nd systematics in Cana Brava and Niquelandia. The extremely low Hf isotope ratios are consistent with contamination from meta-pelitic and calc-silicate rocks found as xenoliths within the LS. The Upper Sequence zircons are characterized by more primitive Hf isotope ratios than the LS and in the scientific community have been largely considered uncontaminated. Our geochemical evaluation and modelling suggests that the US zircons have been affected by contamination from mantle-derived melts, which was masked in the Rb-Sr and Sm-Nd systematics, but in agreement with amphibolite xenoliths presence in the US stratigraphy. The Hf isotope composition of inherited zircons in both LS and US supports this hypothesis, showing negative εHf(t) values in inherited zircons from the LS and positive, mantle-derived εHf(t) values in inherited zircons from the US.

Graphical Abstract (for review)

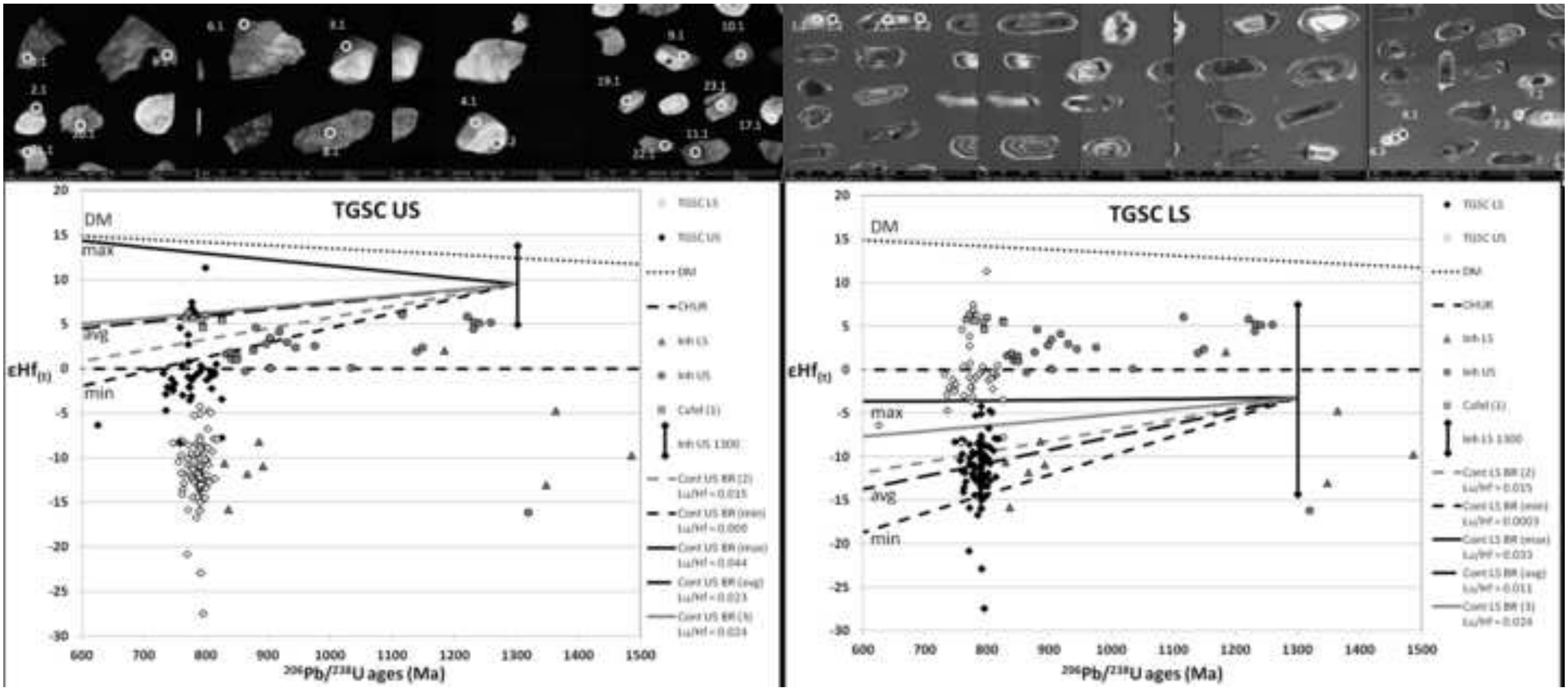

***Highlights (for review)**

Highlights

- Lu-Hf systematics of zircons from the Tonian Goias Stratiform Complex
- Contaminants have crustal affinity in the LS and MORB-like affinity in the US
- Hf isotopes reveal interaction between melts and rocks with similar affinity

*Manuscript
Click here to download Manuscript: manuscript_Lithos.docx Click here to view linked References

The Tonian Goias Stratiform Complex: Lu-Hf isotopes evidences of crustal MORB contamination in mantle-derived melts.

Tommaso Giovanardi[1,2], Maurizio Mazzucchelli[2], Federico Lugli[2], Vicente A.V. Girardi[1], Ciro T. Correia[1], Colombo C.G. Tassinari[1], Anna Cipriani[2,3].

1 Instituto de Geociências, Universidade de São Paulo, Rua do Lago 562, Cidade Universitária, B-05508-900, São Paulo, Brazil; c.a.: maurizio.mazzucchelli@unimore.it

2 Dipartimento di Scienze Chimiche e Geologiche, Università di Modena e Reggio Emilia, Via Campi 103, I-41125 Modena, Italy;

3 Lamont Doherty Earth Observatory of Columbia University, Palisades, New York, 10964, USA.

Abstract

The Cana Brava, Niquelândia and Barro Alto complexes (Goiás, central Brazil) are three of the largest mafic-ultramafic layered complexes in the world. Recent geochemical, geochronological and structural evidences have constrained their origin from a single intrusion (i.e. the Tonian Goias Stratiform Complex), however, still debated is the style and source of contamination of the two sequences that characterize the complex. New in situ Lu-Hf zircon data suggest a strong crustal contamination of the Lower Sequence, but coherent with literature bulk-rock Rb-Sr and Sm-Nd systematics in Cana Brava and Niquelandia. The extremely low Hf isotope ratios are consistent with contamination from meta-pelitic and calc-silicate rocks found as xenoliths within the LS. The Upper Sequence zircons are characterized by more primitive Hf isotope ratios than the LS and in the scientific community have been largely considered uncontaminated. Our geochemical evaluation and modelling suggests that the US zircons have been affected by contamination from mantle-derived melts, which was masked in the Rb-Sr and Sm-Nd systematics, but in agreement with amphibolite xenoliths presence in the US stratigraphy. The Hf isotope composition of inherited

zircons in both LS and US supports this hypothesis, showing negative εHf(t) values in inherited zircons from the LS and positive, mantle-derived εHf(t) values in inherited zircons from the US.

Keywords

layered complex; contamination; Lu-Hf; zircon; Goias

Introduction

The Tonian Goias Stratiform Complex (TGSC hereafter) is a large intrusion discontinuously outcropping along c.a. 350 km in a NNE trend within the Brasilia Belt (northern Goias, central Brasil; Giovanardi et al., 2017a, b). It consists of three major fragments (formerly known as Barro Alto, Niquelândia and Cana Brava, from S to N), only recently identified as one large intrusive event (Giovanardi et al., 2017a, b).

A longstanding debate exists over the degree of contamination of the lower and upper sequences (LS and US hereafter) of the TGSC. While the LS is formed by ultramafics and gabbros showing increasing crustal contamination along the stratigraphy (Correia et al., 1997, 2012; Rivalenti et al., 2008; Giovanardi et al., 2017a), the US consists of anorthosites and olivine-gabbros and is considered uncontaminated (Rivalenti et al., 2008; Correia et al., 2012). This difference between the two units has generated two opposite models of formation: the two-intrusions model, where the LS and US are considered separated intrusions of Neoproterozoic and Mesoproterozoic ages, respectively (Pimentel et al., 2004, 2006; Ferreira Filho et al., 2010; Della Giustina et al., 2011) and the one-intrusion model, in which the US crystallized from an anorthositic melt segregated from the precipitation of the LS ultramafics (Rivalenti et al., 2008; Correia et al., 2012; Giovanardi et al., 2017b).

Literature Sr and Nd isotope ratios show a general increase of crustal contamination along the LS, reaching its maximum in correspondence of the LS top ($^{87}Sr/^{86}Sr_{(t)}$ from 0.706605 up to 0.736590;

$\varepsilon Nd_{(t)}$ from 1.7 down to -8.5; Correia et al., 1997, 2012; Giovanardi et al., 2017a), where dispersed xenoliths from the country metavolcanic-metasedimentary sequence are common (Girardi and Kurat, 1982; Girardi et al., 1981, 1986; Correia et al., 2012; Giovanardi et al., 2017a). Conversely, along the US stratigraphy the Sr and Nd isotopes show almost costant values with mantle-derived affinities and have led to the idea that these are mantle values and therefore the US is not contaminated ($^{87}Sr/^{86}Sr_{(t)}$ from 0.702034 up to 0.704293; $\varepsilon Nd_{(t)}$ from 8.0 down to 4.9; Rivalenti et al., 2008; Correia et al., 2012). However, several metabasaltic and amphibolitic xenoliths are dispersed in the sequence and this led us to believe that also the US must be contaminated. Therefore, new Lu-Hf isotopic analyses of zircons were carried out to constrain the contamination of LS and US in the three fragments of the TGSC. Analyses were also performed on previously SHRIMP U-Pb dated zircons from Giovanardi et al. (2017b) and Correia et al. (2007, 2012). Moreover, new U-Pb and trace elements analyses were carried out to evaluate chemical variations between inherited and magmatic zircons and to expand the U-Pb dataset on poorly-evaluated samples.

Geological setting

The Tonian Goias Stratiform Complex (TGSC) is formed by three separated layered mafic-ultramafic intrusions known as Barro Alto, Niquelândia and Cana Brava complexes outcropping in the Goiás state (central Brazil). The TGSC forms a c.a. 350 km discontinuous belt with NNE direction within the Brasilia Belt (Fig. 1) and is part of the Goiás Massif. This is an exotic terrane, or microcontinent, disrupted and accreted to the São Francisco craton during the Neoproterozoic Brasiliano/Panafrican event that led to the formation of the Gondwana supercontinent (Brito Neves and Cordani, 1991; Pimentel and Fuck, 1992; Fuck et al., 1994; Pimentel et al., 2000).

The TGSC overthrusts to the E the rocks of the Rio Maranhão Thrust Zone, and to the W it is in magmatic contact with a metavolcanic-metasedimentary sequence. The latter is named as Palmeirópolis, Indaianópolis and Juscelândia when in contact respectively with Cana Brava, Niquelandia and Barro Alto (Figs. 2, 3 and 4). The TGSC has a lopolitic structure, thicker in its center (in correspondence of the Niquelandia and the N-S trending part of Barro Alto), where more differentiated units otcrop at its roof, and thinner/tending to disappear at the edges (Cana Brava and the E-W trending part of Barro Alto). The TGSC stratigraphy is divided in two major sequences: the Lower Sequence (i.e. LS), which is common to all fragments, and the Upper Sequence (i.e. US), which outcrops only in Niquelandia and in the N-S portion of Barro Alto.

Starting from the E, the LS of the TGSC is made up by the following units (Figs. 2, 3 and 4):

i) Lower Mafic Zone (LMZ), formed by gabbros mainly recrystallized in micro and mylonitic textures and/or epidote-bearing amphibolites. The recrystallization of this unit is interpreted to be the consequence of the tectonic emplacement of the complexes over the Rio Maranhão Thrust Zone, with a pervasive percolation of fluids in the lower units of the TGSC (Girardi et al., 1986; Correia and Girardi, 1998; Correia et al., 1999; Biondi, 2014).

ii) Ultramafic Zone (UZ), formed by serpentinites interlayered with amphibolites and subordinated gabbros and pyroxenites. Serpentinites and amphibolites originated from the percolation of fluid within peridotites (serpentinites) and pyroxenites, and gabbros (amphibolites). Primary cumulus textures are commonly preserved in these rocks. Approaching the top of the unit, the recrystallization decreases and pyroxenites become predominant. The top of the unit consists of pyroxenites (mainly websterites and subordinate orthopyroxenites) interlayered with gabbros. The transition to the upper unit is characterized by an increase of gabbros and decrease of pyroxenite layers.

iii) Mafic Zone (MZ), formed by gabbros, gabbro-norites and norites. Hydrous minerals (i.e. amphibole and biotite) abundance increases discontinuously along the stratigraphy, reaching its maximum at the top of the unit (named by Girardi et al., 1986, as the 'Hydrous Zone' in Niquelândia). Discontinuous outcrops of diorites, sometimes containing garnet, occur in the sequence. Rocks of this unit are commonly recrystallized and show a foliation parallel to the TGSC direction. Recent studies have demonstrated that this super-imposed foliation formed during the cooling of the TGSC, from hyper- to sub-solidus, under deformative conditions. In this unit, xenoliths from the upper metavolcanic-metasedimentary sequence occur. The first xenolith occurrence consists of decametres-long quartzite layers parallel to the foliation of the TGSC, recognized in both Niquelândia and Cana Brava. Along the stratigraphic succession, xenoliths diminish their dimensions and change in composition. They are amphibolites, garnet-bearing amphibolites, gneisses, metapelite and calc-silicate rocks. Xenoliths maximum abundance is at the top of the MZ (Correia et al., 2012; Giovanardi et al., 2017a).

The US is organized in the following units:

iv) Upper Gabbro-Anorthosite Zone (UGAZ), formed by olivine gabbros grading into anorthosites and troctolites with local occurrence of layers and lenses of subophitic coarse grained isotropic gabbros.

v) Upper Amphibolite (UA), formed by amphibole-bearing gabbros interlayered with amphibolites, epidote-bearing gneisses and/or other lithologies of the metavolcanic-metasedimentary country sequences.

The contact with the stratigraphic upper metavolcanic-metasedimentary sequences (i.e. Palmeirópolis, Indaianopólis and Juscelândia) is magmatic in all the complexes and in both LS and US (Girardi and Kurat, 1982; Girardi et al., 1986; Correia and Girardi, 1998; Ferreira Filho et al., 2010).

The Palmeirópolis, Indaianopólis and Juscelândia sequences are considered fragments of the same crustal sequence (Ferreira Filho et al. 2010 and references therein), showing similar stratigraphy and lithologies. Among the three, the Palmeirópolis Sequence, in contact with Cana Brava, is the largest (c.a. 80 km long and up to 35 km wide).

This crustal unit is formed by successions of metasedimentary rocks (i.e. metacherts, metapelites and calc-silicate rocks) with interbedded metavolcanics (i.e. amphibolites, gneisses and intrusive and sub-volcanic granites; Brod and Jost 1991; Araújo et al. 1995; Araújo 1996; Moraes and Fuck 1994, 1999; Moraes et al. 2003, 2006; Ferreira Filho et al. 2010). The metavolcanics have a compositional variability, from E-MORB to N-MORB geochemical affinity, interpreted to suggest a transitional setting from a continental rift to an aborted ocean basin (Araújo, 1996; Moraes et al. 2003, 2006). Geochronological data on the metavolcanic rocks point to a Mesoproterozoic age between 1.26-1.30 Ga for the magmatic event (Pimentel et al., 2000; Moraes et al., 2006; Ferreira Filho et al., 2010). Rocks of the crustal sequence show a metamorphic recrystallization from greenschist-facies in the W to amphibolite-facies, locally up to granulite-facies, near the contacts with the TGSC (Moraes and Fuck, 1994; Araújo 1996; Moraes et al. 2003, 2006; Ferreira Filho et al. 2010).

Samples

4 samples from Cana Brava, 3 from Barro Alto and 3 from Niquelândia were selected for analyses in zircons of the Lu-Hf and U-Pb isotope systematics. Some of these samples were already investigated for U-Pb analysis (Correia et al., 2007, 2012; Giovanardi et al., 2015, 2017b). When possible, Lu-Hf analyses were carried out onto the same crystals and domains analyzed for U-Pb. The sample list, with position and references, is reported in Table 1.

Samples from Cana Brava (named CB) are three gabbros (samples CB1100, CB1175 and CB1382) and one diorite (sample CB1030) from the LS (Fig. 2). U-Pb SHRIMP ages from the three samples were discussed in Giovanardi et al. (2017b). Samples CB1175 and CB1382 are hydrous granoblastic gabbros with foliation parallel to the complex direction derived by the alignment of pyroxenes and plagioclases. Amphibole is the most abundant hydrous phase and is often associated with biotite. K-feldspar and quartz are minor phases and apatite, spinel and zircon are accessories. Sample CB1100 is a non-foliated gabbro. Differently from the others, it is almost anhydrous, containing only minor amounts of amphibole, but it is enriched in spinel. Diorite sample CB1030 is enriched in orthopyroxene, K-feldspar and quartz with respect to the gabbros. Biotite is the major hydrous phase while amphibole occurs as accessory together with apatite, titanite and zircon.

Zircons from Cana Brava samples commonly show sub-euhedral habits and cathodoluminescence (CL hereafter) internal structures with black cores and a brighter magmatic oscillatory zoning (Giovanardi et al., 2017b). Sometimes bright rim domains with superimposed accretion reabsorb the oscillatory zoning. Anhedral zircons are rare and commonly show irregular chaotic zoning and superimposed domains (Giovanardi et al., 2017b).

Samples from Niquelandia (named NQ) are one gabbro from the LS (sample NQ1549) and two anorthosites from the US (samples NQ1551 and NQ1552). The latter have been previously sparingly dated by U-Pb SHRIMP (Correia et al., 2012 sample NQ1551, and Correia et al. 2007 sample NQ1552). Sample NQ1549 is a foliated hydous grabbro from the top of the LS, outcropping near a gneiss septa, and with a granoblastic texture (Fig. 3). Amphibole is the major hydrous phase while biotite is accessory together with spinel and zircon. εNd(t) value at -6.3 shows crustal contamination (Correia et al., 2012). Samples NQ1551 and NQ1552 are anorthosites with granoblastic texture. They are formed by c.a. 95 % by Vol. of plagioclase with minor amount of amphibole, epidote, scapolite and zircon.

Zircons from sample NQ1549 are similar to those from the Cana Brava gabbros. Description is provided in the 'Results' chapter together with zircons from sample NQ1552. Zircons from sample NQ1551 were divided in three groups (Correia et al., 2012): i) rounded anhedral zircons and xenocrystal cores, ii) euhedral to sub-euhedral crystals with rhythmic zoning or domains and iii) fragments.

Samples from Barro Alto (named BA) are one gabbro (sample BA06T) from the LS and two anorthosites (samples BA01T and BA1541) from the US (Fig. 4). U-Pb SHRIMP data from samples BA06T and BA01T are reported in Giovanardi et al. (2017b) while seven analyses are reported for sample BA1541 by Correia et al. (2007). Sample BA06T is a coarse-grained stratified hydrous gabbro. Stratification is parallel to the complex direction and is formed by the alternance of pyroxenes and amphibole layers with plagioclase layers (Giovanardi et al., 2017b). Spinel is abundant in the femic layers while zircon occurs as accessory. Samples BA01T and BA1541 have granoblastic textures and plagioclase is more than 90% by Vol (Correia et al., 2007). Minor amounts of clinopyroxene and amphibole occur as interstitial phases along deformative structures (Giovanardi et al., 2017b). Apatite, rutile, epidote and zircon occur as accessory phases.

Zircons from sample BA06T are euhedral to sub-euhedral, with commonly dark cores and magmatic oscillatory zoning/domains in CL. Rim zoning is commonly brighter than cores. Zircons from sample BA01T are commonly anhedral, with few crystals sub-euhedral. CL internal structures are commonly erased, appearing as homogeneous grey areas, while in few grains a dark core is surrounded by chaotic overgrowth structures.

Analytical methods

Zircons were separated after crushing, milling, magnetic and heavy liquid separation, and hand picking and embedded in resin. After Au-coating, the polished mounts were comprehensively examined with a FEI-QUANTA 250 scanning electron microscope equipped with secondary-electron and cathodoluminescence (CL) detectors at IGc-CPGeo-USP; the most common conditions used in CL analysis were 60 μA of emission current, 15.0 kV of accelerating voltage, 7 μm of beam diameter, 200 μs of acquisition time, and a resolution of 2048x1887 pixels and 345 dpi. Some samples were also analyzed by the U-Pb isotopic technique using a SHRIMP-IIe machine also at IGc-CPGeo, Universidade de São Paulo, following the analytical procedures presented in Williams (1998). Correction for common Pb was made based on the ^{204}Pb measured, and the typical error component for the ^{206}Pb/^{238}U ratio is less than 2%; U abundance and U-Pb ratios were calibrated against the TEMORA-II standard. The dataset consists of 56 U-Pb SHRIMP-II analyses and is reported in Supplementary Material A. 24 analyses were performed on zircons from the US anorthosite of Barro Alto (sample BA1541) and 32 analyses were carried on zircons from Niquelândia, 16 for sample NQ1549 (a gabbro from the top of the LS) and 16 for sample NQ1552 (an anorthosite from US). For all samples, ^{207}Pb/^{235}U and ^{206}Pb/^{238}U concordia age (with 95% of confidence level and 2σ error) are calculated using Isoplot© 4.1 software (Ludwig, 2009).

In situ Lu–Hf isotope analyses were performed at the Centro Interdipartimentale Grandi Strumenti (CIGS) of the University of Modena and Reggio Emilia (Italy) using a double focusing MC–ICP-MS with a forward Nier–Johnson geometry (Thermo Fisher Scientific, Neptune™), coupled to a 213 nm Nd:YAG laser ablation system (New Wave Research™).

During the analytical session, two zircon reference materials (TEMORA-2 and CZ3) were employed to check the accuracy and the precision of the measurements. Eight of nine Faraday detectors were used to collect the following masses: 171Yb, 173Yb, 175Lu, 176Hf+Lu+Yb, 177Hf, 178Hf, 179Hf, 180Hf.

Laser data were acquired in static mode with a block of 250 cycles (including laser warm-up, ~50–80 cycles of analysis and wash-out), an integration time of 0.5 s, a laser spot of 55 µm and a fluence of ~10 J/cm^2. A low laser frequency (~10 Hz) was used to achieve a better signal stability (Vroon et al. 2008) with a He flux of ~0.5 L/min. Before each analysis, the surface of the zircon was pre-ablated with a spot size of 60 µm.

Data reduction was performed with the Hf-INATOR excel spreadsheet (Giovanardi & Lugli, 2017). TEMORA-2 yielded a ^{176}Hf/^{177}Hf ratio of 0.282689 ± 0.000080 (2σ; n = 37), identical within the error to the reference value of 0.282693 (Matteini et al., 2010); similarly, CZ3 yielded a ^{176}Hf/^{177}Hf ratio of 0.281722 ± 0.000027 (2σ; n = 20; reference value: 0.281729; Wu et al., 2006). The entire dataset resulting from the analyses of our zircon samples consists in 145 analyses reported in Supplementary Material B and average of magmatic and inherited zircons for each sample are reported in Table 2. When possible, Lu-Hf analyses were carried out within the same domain of U-Pb analyses. Lu-Hf data have been recalculated to 790 Ma, considering this age as the best representative for the complexes intrusion. Data were recalculated using the $(^{176}\mathrm{Hf}/^{177}\mathrm{Hf})_{CHUR}$ and $(^{176}\mathrm{Lu}/^{177}\mathrm{Hf})_{CHUR}$ present-day values as 0.282772 and 0.0332 from Blichert-Toft and Albarede (1997).

U-Pb in situ analyses were also replicated at the CIGS of the University of Modena and Reggio Emilia on several zircons already investigated through SHRIMP analyses. Analyses were carried out coupling the laser ablation system to a quadrupole ICP-MS X Series II (Thermo Fisher Scientific) and employing a laser spot size of 40 μm, a repetion rate of 10 Hz and a fluence of 10 J/cm^2. The IPC-MS was tuned using NIST612 glass reference material to optimize the signal intensity and stability, checking ^{139}La, ^{238}U and the ^{238}U/^{232}Th ratio. The oxide production within the plasma was monitored employing the ^{232}Th^{16}O/^{232}Th ratio, constantly kept below 0.01%. Acquired masses were 202Hg, 204Pb(+204Hg), 206Pb, 207Pb, 208Pb, 232Th, 235U and 238U. ^{206}Pb/^{207}Pb, ^{207}Pb/^{235}U and ^{206}Pb/^{238}U ratios were calculated during the analyses. TEMORA-2 and CZ3 were used as known and unknown (respectively) zircon reference materials and bracketed during the analysis. Sample U-Pb ratios were thus corrected for laser induced elemental fractionation using TEMORA-2 as reference. Analyses are reported in Supplementary Material A.

Trace element analysis was performed at the CIGS using the same instrumental condition presented for U-Pb determination (e.g. Lugli et al., 2017a; Sforna and Lugli, 2017). The system is equipped with a collision-reaction cell to drastically attenuate polyatomic interferences. Si, Ti, REE and Hf were thus acquired within two analytical sessions. Elemental quantification was performed using NIST 610, 612 and 614 as reference materials and Si as internal standard, previously measured by ion microprobe. Resulting RSD for all the trace element data is always better than 10%. Data are reported in Supplementary Material C.

Sr isotopes analyses were determined for 2 samples (Table 3). Plagioclases were handpicked under a microscope and leached, dissolved and separated using standard techniques. The ^{87}Sr/^{86}Sr ratios were measured as 200 ppb solutions by MC-ICP-MS on a Thermo Scientific Neptune housed at the CIGS UNIMORE. Samples and standards were analysed in a static multi-collection mode in a single block of 100 cycles with an integration time of 8 seconds per cycle. The instrumental mass fractionation was corrected for by using a stable isotopic ^{86}Sr/^{88}Sr ratio of 0.1194 and an exponential law. Repeated analyses of the NBS-987 reference material yielded a mean ^{87}Sr/^{86}Sr ratio of 0.710270 ± 0.000010 (2σ; n = 4). The ^{87}Sr/^{86}Sr ratios were corrected for instrumental bias to an accepted value for the NBS-987 of 0.710260.

In situ Sr isotope analyses were performed at the CIGS using the 213 nm laser ablation system and the Neptune MC-ICP-MS (Lugli et al., 2017b). Laser ablation parameters were the same of Hf isotope analyses. We collected the same masses of the dissolution analyses plus mass 85.5 and 86.5 to check for the doubly charged Yb intereference. Background Kr was corrected measuring 60 s of gas blank with laser switched off. The presence of Ca dimers and argides was also monitored on mass 82 after the Kr subtraction. Isobaric Rb was corrected as for the dissolution analysis. The instrument was tuned for the maximum sensitivity on mass 88, but also checking the accuracy of the $^{87}Sr/^{86}Sr$ ratio of an in-house reference material (modern marine shell), which yielded a Sr isotopic ratio of 0.709166 ± 0.000039 (2σ; n = 4), in agreement with modern seawater (0.70917). International reference material JCt-1 was also analyzed yelding a $^{87}Sr/^{86}Sr$ ratio of 0.709151 ± 0.000013 (2σ; n = 4). Analyses are reported in Table 3.

Results

Plagioclase Sr isotopes

Plagioclase from gabbro BA06T (LS) and anorthosites BA01T (US) and BA02T (US) have an average Sr concentration of 164 ± 8 ppm, 151 ± 8 ppm and 148 ± 9 ppm, respectively, calculated on 30 LA-ICP-MS analyses each. Rb average concentration is 0.5 ± 0.4 ppm in sample BA06T, 0.2 ± 0.1 ppm in sample BA01T and 0.3 ± 0.4 ppm in BA02T, with Rb/Sr ratios of 0.0030, 0.0011 and 0.0020, respectively.

LS gabbro BA06T show a solution $^{87}Sr/^{86}Sr$ ratio of 0.729226 ± 0.000012 and an in situ $^{87}Sr/^{86}Sr$ ratio of 0.729948 ± 0.000125 (2σ; average of 3 analyses). The solution $^{87}Sr/^{86}Sr$ ratio of US anorthosite BA02T is 0.702368 ± 0.000012, the in situ $^{87}Sr/^{86}Sr$ is 0.702444 ± 0.000329 (2σ; average of 3 analyses). US anorthosite BA01T was not analysed in solution, but the in situ $^{87}Sr/^{86}Sr$ ratio is 0.702452 ± 0.000040 (2σ; average of 2 analyses), consistent with anorthosite BA02T. Recalculated $^{87}Sr/^{86}Sr$ ratios at 790 Ma provide $^{87}Sr/^{86}Sr_{(790)}$ ratios of 0.729192 and 0.729914 (in solution and in situ, respectively) for gabbro BA06T, of 0.702355 and 0.702432 (in solution and in situ, respectively) for anorthosite BA02T and of 0.702430 (in situ) for anorthosite BA01T.

The Sr isotope ratios of LS gabbro BA06T are consistent with literature bulk-rock data from the upper MZ (i.e. the Hydrous Zone) of Cana Brava and Niquelandia, with $^{87}Sr/^{86}Sr_{(790)}$ ratios between 0.721461 and 0.736590 (Correia et al., 2012; Giovanardi et al., 2017a; Fig. 5). Similarly, Sr isotopes from US anorthosites BA01T and BA02T are consistent with bulk rock literature data from the Niquelandia US, with $^{87}Sr/^{86}Sr_{(790)}$ ratios between 0.702243 and 0.702839 (Correia et al., 2012; Fig. 5).

U-Pb zircon geochronology

Barro Alto US anorthosite (sample BA1541)

Sample BA15-41 is an anorthosite from the Barro Alto US located near the contact with the Juscelandia Sequence. Zircons from sample BA1541 could be divided in two groups. The first includes anhedral to sub-euhedral extremely fractured zircons which in CL show almost homogeneous medium emission suggesting a complete recrystallization (Fig. 6). The second group is formed by anhedral crystals which in CL show extremely bright core domains and a discordant darker rim growth with poor or no zonation (Fig. 6).

Twentyfour U-Pb analyses were performed on 23 zircons from sample BA1541. Zircons from sample BA1541 yielded twenty one concordant ages ranging between 863 ± 15 Ma and 731 ± 26 Ma ($^{206}Pb/^{238}U$ single spot age, 1σ error), with a weighted average of 774 ± 12 Ma (95% confidence error level, MSWD = 2.2; Fig. 6) and a concordia age of 780 ± 10 Ma (95% confidence error level, decay-const. errs included, MSWD = 0.48, probability of concordance = 0.49; Fig. 6). Two discordant ages were discarded, but fall within the range. One older concordant $^{206}Pb/^{238}U$ single spot age of 1034 ± 19 Ma was also obtained.

Niquelândia LS gabbro (sample NQ1549)

Zircons from sample NQ1549 are euhedral to sub-euhedral and commonly show an oscillatory magmatic zonation in CL (Fig. 7). This zonation is sometimes truncated by a discordant, thin bright rim (Fig. 7). Few zircons show an inherited core commonly bright and unzoned in CL (Fig. 7).

Sixteen analyses were performed on 7 zircons. Eleven analyses yielded concordant ages ranging between 793 ± 11 Ma and 759 ± 10 Ma ($^{206}Pb/^{238}U$ single spot age, 1σ error), with a weighted average of 771 ± 8 Ma (95% confidence error level, MSWD = 1.5; Fig. 7) and a concordia age of 772 ± 6 Ma (95% confidence error level, decay-const. errs included, MSWD = 2.8, probability of concordance = 0.09; Fig. 7). A younger discordant analysis gave a $^{206}Pb/^{238}U$ single spot age at 756 ± 16 Ma. Four concordant analyses from inherited cores provide for older $^{206}Pb/^{238}U$ single spot ages between 1364 ± 24 Ma and 1063 ± 21 Ma.

Niquelândia US anorthosite (sample NQ1552)

Zircons are anhedral to sub-euhedral and are commonly fractured. Similar to sample BA1541, two different groups are defined with CL images: the first is characterized by unzoned, extremely bright crystals and the second by poor or unzoned crystals with medium emissions and a discontinuous bright rim (Fig. 8).

Fifteen Analyses yielded concordant ages ranging between 975 ± 17 Ma and 762 ± 12 Ma ($^{206}Pb/^{238}U$ single spot age, 1σ error) with a weighted average of 850 ± 33 Ma (95% confidence error level, MSWD = 18). One discordant age falls in the interval.

Lu-Hf zircon data

One-hundred and fortyfive in situ Lu-Hf analyses were performed on zircon grains as follow: fiftytwo analyses on zircons from Cana Brava (CB1030 = 16; CB1175 = 15; CB1382 = 6; CB1100 =15), fortythree analyses on zircons from Niquelândia (NQ1549= 20; NQ1552 = 18; NQ1551 = 5) and fifty analyses on zircons from Barro Alto (BA06T = 20; BA01T = 12; BA1541 = 18). When possible, Lu-Hf analyses were carried out in the same domain of U-Pb SHRIMP analyses.

Otherwise, the Lu-Hf data have been recalculated to 790 Ma, considering this age as the best representative for the complexes intrusion (Giovanardi et al., 2017b).

LS Cana Brava zircons range between εHf(t) -25.1 and -24.8, with an average εHf(t) of -11.68 (Fig. 9). In details, analyses on zircons from LS gabbro CB1175 show $^{176}Hf/^{177}Hf$ ratios between 0.281653 and 0.282153. εHf(t) varies from -12.7 to -4.8 with one single spot showing a lower value at -22.9. Zircons from LS gabbro CB1382 have $^{176}Hf/^{177}Hf$ ratios between 0.281911 and 0.282038 and εHf(t) values between -14.4 and -9.4. $^{176}Hf/^{177}Hf$ ratios in zircons from LS gabbro CB1100 is between 0.281589 and 0.281976. εHf(t) varies between -16.0 to -10.6 with one spot at -25.1. LS diorite CB1030 show$^{176}Hf/^{177}Hf$ between 0.28827 and 0.282058 with εHf(t) values between -16.7 and -8.5.

$^{176}Hf/^{177}Hf$ ratios from the LS Barro Alto gabbro (sample BA06T) range between 0.281824 and 0.282077. εHf(t) values are between -15.8 and -8.3 (Fig. 9). The US Barro Alto anorthosite BA01T show $^{176}Hf/^{177}Hf$ ratios between 0.281523 and 0.282596 with very scattered εHf(t) values ranging from -16.1 to 11.3 (Fig. 9). Conversely, εHf(t) values from US anorthosite sample BA1541 vary between -3.6 and 2.4 (Fig. 9) with $^{176}Hf/^{177}Hf$ ratios between 0.282154 and 0.282313.

Zircons from LS Niquelândia gabbro NQ1549 show $^{176}Hf/^{177}Hf$ ratios between 0.281602 and 0.282194 with scattered εHf(t) values varing from -27.6 and 5.9 (Fig. 9). Mesoproterozoic cores show positive values (εHf(t) = 2.0 and 5.9) and, commonly, less negative values compared to rims. The US anorthosite NQ1552 zircons have $^{176}Hf/^{177}Hf$ ratios between 0.282212 and 0.282363 and εHf(t) values between -3.0 and 4.6 (Fig. 9). The few data from the other US anorthosite, sample NQ1551, are commonly higher ($^{176}Hf/^{177}Hf$ between 0.282439 and 0.282501; εHf(t) between 5.3 and 7.7; Fig. 9) with one value lower than sample NQ1552 ($^{176}Hf/^{177}Hf$ = 0.282070; εHf(t) = -7.7; Fig. 9).

Overall, the LS gabbros from the three complexes show the same εHf(t) range, with values falling below the CHUR array and thus sub-chondritic in composition (Fig. 9). Similarly, zircons from the US samples have mostly overlapping εHf(t) values (Fig. 9). With the exception of zircons from anorthosite NQ1551, samples from US form a decreasing εHf(t) linear trend from older zircons to younger ones (Fig. 9): the εHf(t) values range from positive (older zircons) to slightly negative (younger zircons). With few exceptions, the εHf(t) values of US zircons are less negative than those of the LS samples (Fig. 9).

Zircon trace elements

According to the REE abundances, zircons are classified in magmatic (Hoskin et al., 2005) and continental (according to the U/Yb vs Hf discriminant diagram from Grimes al., 2007). From here, we will use the term 'magmatic' to define those zircons that show ages consistent with the TGSC Neoproterozoic intrusion (i.e. younger than 825 Ma) and with CL structures consistent with their magmatic origin.

Magmatic zircons from the TGSC show, in the LS, large variation of LREE (in the order of 3 orders of magnitude for La, Fig. 10) with respect to HREE (less than 1 order for Lu). US zircons are characterized by LREE abundances commonly lower than LS zircons, with the exception of Ce (Fig. 10). An increase in the La content is accompanied by an increase in REE abundances in both LS and US zircons. Zircons in the two sequences show, with the exception of US anorthosite NQ1551, similar REE patterns with comparable pronounced Eu negative anomalies ($(Eu/Eu^*)_N$ between 0.1 and 0.4). Zircons from US anorthosite NQ1551 have lower ΣREE and less negative Eu anomalies (Fig. 10; $(Eu/Eu^*)_N$ between 0.8 and 1.0). Two similar patterns were found in inherited zircons in the US, both in Niquelandia and Barro Alto (Fig. 10), showing $(Eu/Eu^*)_N$ between 0.9 and 1.3.

One magmatic zircon from Barro Alto US and two inherited zircons from US in both Barro Alto and Niquelandia show flat LREE trends with poor/none Ce anomalies (Fig. 10). Similar REE patterns have been recognized in granitoids zircons (Belusova et al., 2002) and hydrothermal zircons (Hoskin and Schaltegger, 2003; Yang et al., 2014).

Inherited zircons from US commonly show lower REE abundances than inherited zircons from LS (e.g., Lu between 10 and 55 ppm and between 20 and 143 ppm, respectively). LS inherited zircons have higher LREE contents (e.g., La_N between 0.40-3.33 and 0.04-0.34 respectively) and more pronounced Eu negative anomalies ($(Eu/Eu^*)_N$ between 0.07 and 0.49 and between 0.34 and 1.3 respectively).

Discussion

The magmatic affinity of the TGSC

The new Sr isotopes data on plagioclases from the Barro Alto complex show that its US and LS have the same geochemical affinity of Niquelandia and Cana Brava (Fig. 5). These data (together with Nd isotopes from Niquelandia and Cana Brava) suggest that the LS was progressively contaminated during its crystallization by incorporated xenoliths of the upper metavolcanic-metasedimentary sequence. Conversely, the US appears to be uncontaminated, notwithstanding xenoliths occurrences reported in both Niquelandia and Barro Alto (Girardi et al., 1981, 1986; Rivalenti et al., 2008; Correia et al., 2012; Giovanardi et al., 2017a, b), showing Sr isotopic values comparable with mantle-derived melts.

Although this isotopic discrepancy suggests that US and LS could be interpreted as two separate intrusions (i.e. the two-intrusions model; Ferreira Filho et al., 2010; Della Giustina et al., 2011 and references therein), U-Pb zircon chronology provides the same intrusion age for the two sequences (Correia et al., 2007, 2012; Giovanardi et al., 2017b). The new U-Pb data in this work reinforce this interpretation, pointing to a Neoproterozoic intrusion age for the TGSC at ~790 Ma, in agreement with the one-intrusion model (Correia et al., 2007, 2012; Giovanardi et al., 2017b).

Lu-Hf zircon data from the TGSC produce two almost separated εHf(t) fields with US values from slightly negative to positive and much lower LS values (εHf(t) from -8.1 up to 11.3 from US magmatic zircons and from -27.5 up to -4.2 from LS magmatic zircons).

The higher εHf(t) values of the US zircons suggest a more primitive mantle-derived source for the parent melts of the US zircons with respect to the LS zircons. The negative sub-chondritic values of the LS zircons clearly indicate a strong crustal (mainly detritic) component in the parent melt, which is compatible with the crustal contamination observed with Sr and Nd isotopes.

Among the US magmatic zircons, those from anorthosite NQ1551 show the highest εHf(t) (between 5.3 and 7.7, with the exception of one zircon from anorthosite BA1541 with a value of 11.3) and lowest REE abundances (Fig.s 9 and 10). Differently from other US zircons, they show a poor/none Eu negative anomaly ($(Eu/Eu^*)_N$ between 0.8 and 1.0). The absence of Eu anomaly could be related to i) the different f_{O2} condition of the parent melt (Trail et al., 2012) or ii) the zircon crystallization before plagioclase precipitation. The lower REE contents with respect to other zircons suggest the second hypothesis. These features suggest that zircons from anorthosite NQ1551 could be considered as the most primitive among the studied ones, thus reflecting the original isotopic composition of the TGSC parent melt.

Hf isotopic data from other US zircons exhibit εHf(t) values commonly slightly negative (Fig. 9), which suggest that they crystallized from a contaminated melt similar to LS zircons.

The commonly low REE zircons of the US with respect to LS zircons suggest that the US anorthosites formed during the initial stages of the TGSC intrusion considering also that these rocks are formed by >90% of plagioclase and the absence of others HREE-compatible minerals.

The new trace element and isotopic data thus support the hypothesis that the US crystallized from an anorthositic melt formed during the segregation of the ultramafic cumulates (i.e. the UZ) during the first stages of the TGSC intrusion (Rivalenti et al., 2008; Correia et al., 2012).

Given that Hf isotopes are not easily mobilized in zircons (Kinny and Maas, 2003), the consistent behaviour of Sr and Nd isotopes in bulk rock and Hf ratios in zircons suggest that Sr and Nd systematics in the TGSC are dependant from magmatic contamination/primary nature of the parent melt and were poorly/none affected by later events. According to these isotope data and to other field, petrological and geochronological evidences (Correia et al., 2012; Giovanardi et al., 2017a, b), the two-intrusions model with TGSC recrystallization by granulitic- and amphibolite-facies metamorphic events (also with fluids occurrences, Pimentel et al., 2004, 2006; Ferreira Filho et al., 2010; Della Giustina et al., 2011) must be discarded.

Inherited zircons and re-opening processes as revealed from Lu-Hf isotopes

Inherited zircons from LS and US show different elemental and isotopic signatures (Fig.s 9 and 10). Inherited zircons from the LS have higher REE abundances and Eu negative anomaly associated to lower εHf(t) values than US inherited zircons (εHf(t) average of -6.8 and 2.6 respectively) thus suggesting a contamination by a crustal component. These data agree with xenolith occurrences reported in literature, with a stratigraphic variation of xenoliths within the TGSC, from the base of the MZ up to the complex roof. In the MZ, xenoliths are quartzites (near the base of the MZ), meta-pelite, calc-silicatic rocks and subordinate amphibolites (Girardi et al., 1981, 1986; Correia et al., 1997, 2012; Giovanardi et al., 2017a). Xenoliths in the US are amphibolites with subordinate minor amounts of calc-silicatic rocks near the LS-US transition (Girardi et al., 1981, 1986; Correia et al., 1997, 2012; Giovanardi et al., 2017a). Amphibolites have been related to MORB magmatism between 1.26 and 1.30 Ga in connection with the development and abortion of a continental rift (Pimentel et al., 2000; Moraes et al., 2006).

Inherited zircons from US show εHf(t) values recalculated to the age of the MORB magmatic event in the metavolcanic-metasedimentary sequence (i.e. 1.3 Ga) comparable with mantle-derived melts between 5.5 and 13.9 with an average of 9.5 (with the exception of a single zircon at -16.5). As expected, recalculated εHf(t) values at the 1.3 Ga magmatic event of LS inherited zircons point to crustal values with an average of -3.2 showing a wide range between -14.1 and 7.6. This range reflects the lithological variability of the LS xenoliths, while the low xenolith diversity in the US results in a narrow Hf isotope range.

The linear trend formed by the US inherited zircons εHf(t) values with $^{206}Pb/^{238}U$ ages (Fig. 9) suggests that these zircons suffered a re-opening of the system, which caused Pb loss and age rejuvenation (Vervoot and Kempt, 2016). The LS inherited zircons εHf(t) values plotted with U/Pb ages do not show a well-defined trend as for the US inherited zircons. Their lack of data along the time interval between the 1.3 Ga magmatism and the 790 Ma TGSC intrusion could be the result of a more efficient Pb loss process than for the US inherited zircons. This hypothesis is supported by the absence, between the 1.3 Ga magmatism and the TGSC intrusion age, of other recognized magmatic events in the upper metavolcanic-metasdimentary sequence. Moreover, REE trends of inherited zircons in both US and LS are similar to the magmatic ones (Fig. 10), suggesting the re-equilibration of these elements with the TGSC parent melt. In this scenario, the re-opening of the zircon system occurred during the zircon residence in the magmatic chamber.

Conversely, the flat-LREE patterns of few zircons from US, comparable with hydrothermal zircons, suggest re-equilibration processes occurring locally after the TGSC crystallization. The hydrothermal nature of this re-equilibration process, the low number of such zircons and their occurrence only in the US suggest that this process is related to local tectonism (visible in the many faults and shear zones in the area), possibly related to the bending/exhumation of the complex, estimated at c.a. 650 Ma by U-Pb zircon discordant ages and rutile analyses (Ferreira Filho et al., 1994, 1998; Giovanardi et al., 2017b).

Contamination of the TGSC: Lu-Hf isotopes constraints

Rb-Sr and Sm-Nd isotopes suggested that while the LS was strongly contaminated by xenoliths from the metavolcanic-metasedimentary sequence, the US seemed unaffected by contamination (Fig. 5; Rivalenti et al., 2008; Correia et al., 2012). Accordingly, zircon Hf isotopes of the LS and US plot into two almost distinct fields (Fig. 9).

LS Hf zircon isotope ratios are consistent with crustal contamination as shown by other systematics (Fig. 9). Likewise, the LS inherited zircons show negative $\varepsilon Hf_{(t)}$ values, which are consistent with the crustal origin of the contaminants. The Hf isotopic variability of the US zircons provides for positive to negative εHf(t) values and suggests that part of the US suffered contamination similar to

LS: the two fields slightly overlap and provide a unique trend of contamination from the US to the LS (Fig. 9). The commonly slightly negative εHf(t) values of magmatic US zircons (with the exception of sample NQ1551 and few others) do not resemble mantle-derived melts, which usually have positive $\varepsilon Hf_{(t)}$ (Kemp et al., 2006; Hawkeswort and Kemp, 2006). Inherited US zircons also show an evolutionary trend related to the U-Pb system re-opening, which suggest negative $\varepsilon Hf_{(t)}$ values at the time of their incorporation within the US.

Because Hf isotopes are immobile in zircons (Kinny and Maas, 2003), variations in their Hf isotopic composition are constrained by variations in the composition of the melt. The different lithologies of the xenoliths recognized in US and LS suggest that the contamination of the two sequences is related to the contaminant composition: continental/detrital crustal contaminant for the LS, where xenoliths are meta-sedimentary rocks, and MORB-like contaminant for the US, where xenoliths are amphibolites related to mantle-derived melts.

As discussed above, zircons from anorthosite NQ1551 show the most primitive geochemical and Hf isotopic features and could be considered as a proxy of the uncontaminated Hf isotopic values of the TGSC parent melt.

Considering the $^{176}Hf/^{177}Hf_{(t)}$ of inherited zircons as a proxy of the initial Hf isotopic value of the rock at its time of formation we calculated the average $^{176}Hf/^{177}Hf_{(1300)}$ of inherited zircons as the bulk rock contaminant, which averages at 0.281866 for LS and at 0.282224 for the US (Fig. 11). For the US average calculation, a single zircon with $^{176}Hf/^{177}Hf_{(1300)}$ of 0.281490 and $\varepsilon Hf_{(1300)}$ of -16.5 ($^{206}Pb/^{238}U$ age at 1319 Ma) was discarded as clearly inherited from a detritical/sedimentary rock. Metasedimentary xenoliths can also be found in the US, however, they are largely subordinated to amphibolites.

Contaminants in the LS are mainly metasediments whose ages are still uncertains. To better compare the data and evolution trends between LS and US contaminants, we recalculated the $^{176}Lu/^{177}Hf_{(t)}$ of the contaminants at the age of the MORB volcanic activity in the country sequence (i.e., the age of formation of amphibolites) at 1.3 Ga (Moraes et al., 2003, 2006). The $^{176}Lu/^{177}Hf$

ratio of the bulk rock of the contaminants was extimated using the Bulk Continental Crust of 0.015 (Griffin et al., 2002) and the average of MORB at 0.024 (Stracke et al., 2003) for both sequences (Fig. 11). For the LS, evolution trends for the contaminant bulk rock were also calculated using $^{176}Lu/^{177}Hf$ ratios obtained from bulk rock analyses of the LS metasedimentary xenoliths ($^{176}Lu/^{177}Hf$ min = 0.0003, max = 0.033 and avg = 0.011; recalculated data using the 0.1419 constant of conversion from Blichert-Toft et al., 1998; bulk rock analyses from Correia et al., 2012). For the US, $^{176}Lu/^{177}Hf$ ratios were obtained from bulk rock analyses of the amphibolites of the metavolcanic-metasedimentary sequence ($^{176}Lu/^{177}Hf$ min = 0.009, max = 0.044 and avg = 0.023; bulk rock analyses from Moraes et al., 2003). The similarities between the $^{176}Lu/^{177}Hf$ average ratios calculated for the US and LS contaminants with the average MORB and Bulk Continental Crust are consistent with contamination processes in both sequences, but with different lithologies.

Average bulk rock contaminants calculated for LS show $\varepsilon Hf_{(790)}$ between -14.5 and -3.6 with an average of -10.9 at the time of the TGSC intrusion, including almost all the $\varepsilon Hf_{(790)}$ of magmatic zircons (Fig. 11). The more crustal values from few LS magmatic zircons can be modelled by using the lowest $^{176}Hf/^{177}Hf_{(1300)}$ of 0.281560 from LS inherited zircons which provides $\varepsilon Hf_{(790)}$ of the contaminants between -25.3 and -14.4 with an average of -21.7. The absence of inherited domains in these zircons, as shown by CL investigation, suggests their crystallization from an extremely contaminated melt if not directly from a melt derived from the contaminant itself.

Average bulk rock contaminants calculated for US at the time of the TGSC intrusion show $\varepsilon Hf_{(790)}$ between 1.1 and 13.0 with an average of 5.9. These values are higher than most of the TGSC magmatic zircons (Fig. 11). Recalculating the contaminants bulk rock using the lowest MORB-like $^{176}Hf/^{177}Hf_{(1300)}$ of 0.282112 (i.e. the lower recalculated inherited zircon for the US was at 0.281490) provides $\varepsilon Hf_{(790)}$ values between -2.9 and 9.0 with an average of 1.9, which comprise almost all the US magmatic zircons. Six US magmatic zircons with $\varepsilon Hf_{(t)}$ between -3.0 and -8.4 require a more detrital/sedimentary component, which is however compatible with the rare occurrence of these xenoliths and related inherited zircons.

The Hf isotopic data from zircons thus provide a valuable tool to recognize contamination processes between melt and rock with similar original isotopic compositions, which could not be identified with other bulk-rock isotopic systematics (i.e. Rb-Sr and Sm-Nd). Similarly, the occurrences in magmatic systems of magmatic and inherited zircons could be used to qualitatively recognize contamination processes and approximate the contaminant Hf isotopic composition when xenoliths/contaminat bulk rock is missing.

Conclusions

The emplacement and contamination of the TSGC complex within crustal units has been clearly recorded by Lu-Hf systematics in zircons from both the LS and the US sequences of its three fragments (Niquelandia, Cana Brava and Barro Alto).

The intrusion of the LS within the metasedimentary sequence has resulted in a clear crustal signature (negative εHf(t) zircon values), coherent with bulk-rock Rb-Sr and Sm-Nd isotopes.

The emplacement of the US at shallower crustal levels, dominated by MORB-mantle like signature amphibolites, resulted in zircon εHf(t) values from slightly positive to negative. The similar original geochemical affinities of the TGSC parent melt and amphibolites masked the contamination processes in the US in the Rb-Sr and Sm-Nd bulk-rock systematics leading over the years to an erroneous geotectonic interpretation of the US. Zircon Hf isotopes record the interaction between the TGSC parent melt and the evolved MORB-like signature of the contaminant from the adjacent metavolcanic sequence.

The LS and US were, thus, similarly contaminated during the TGSC intrusion, resulting in different geochemical affinities due to the different composition of the contaminants.

The occurrences of un/poorly contaminated zircons in the US suggest that anorthosites crystallized from an anorthosithic crystal mush, which was formed during the segregation of the ultramafics in the initial stage of the TGSC intrusion.

Acknowledgements

This work was supported by FAPESP (Fundação de Amparo à Pesquisa do Estado de São Paulo) in the frame of project 2013/19519-6.

Analytical facilities and their development have benefited of the MIUR PRIN 2015 Prot. 20158A9CBM_005 and Programma Giovani Ricercatori "Rita Levi Montalcini".

References

Anders, E., Edibara, M., 1992. Solar system abundances of the elements. Geochimica and Cosmochimica Acta 46, 2363-2380.

Araújo, S.M., Fawcett, J.J., Scott, S.D., 1995. Metamorphism of hydrothermally altered rocks in a volcanogenic massive sulfide deposit: the Palmeirópolis, brazil, example. Revista Brasileira de Geociências 25(3), 173-184.

Araújo, S.M., 1996. Geochemical and isotopic characteristics of alteration zones in highly metamorphosed volcanogenic massive sulfide deposits and their potential application to mineral exploration. Unpublished Ph.D. Thesis, Department of Geology, University of Toronto, Canada, 210.

Belusova, E.A., Griffin, W.L., O'Reilly, S.Y., Fisher, N.I. 2002. Igneous zircon: trace element composition as an indicator of source rock type. Contributions to Mineralogy and Petrology 143, 602-622.

Biondi, J.C., 2014. Neoproterozoic Cana Brava chrysotile deposit (Goiás, Brazil): Geology and geochemistry of chrysotile vein formation. Lithos 184-187, 132-154.

Blichert-Toft, F., Albarede, F., 1997. The Lu–Hf isotope geochemistry of chondrites and the evolution of the mantle–crust system. Earth and Planetary Science Letters 148, 243–258.

Blichert-Toft, F., Albarede, F., Gleason, J.D., Kring, D.A., Hill, D.H., Boynton, W.V., 1998. Lu-Hf isotopic compositions of SNC meteorites: Implications for Martian mantle evolution. Goldschmidt conference abstract, in Mineralogical Magazine 62A.

Brito Neves, B.B., Cordani, U.G., 1991. Tectonic evolution of South America during the late Proterozoic. Precambrian Research 53, 23–40.

Brod, J.A., Jost, H., 1991. Características estruturais, litológicas e magmáticas da zona de cisalhamento dúctil do Rio Traíras, bloco do Complexo Niquelândia, Goiás. Revista Brasileira de Geociências 21, 205-217.

Correia, C.T., Girardi, V.A.V., 1998. Geoquimica e petrologia das rochas maficas e ultramaficas do complexo estratiforme de Cana Brava - GO, e das suas encaixantes. Boletim de Instituto de Geociências USP 29, 1-37.

Correia, C.T., Girardi, V.A.V., Tassinari, C.G., Jost, H., 1997. Rb-Sr and Sm-Nd geochronology of the Cana Brava layered mafic-ultramafic intrusion, Brasil, and considerations regarding its tectonic evolution. Revista Brasileira de Geociências 27(2), 163-168.

Correia, C.T., Jost, H., Tassinari, C.C.G., Girardi, V.A.V., Kinny, P.D., 1999. Ectasian Mesoproterozoic U–Pb ages (SHRIMP II) for themetavolcano-sedimentary sequences of Juscelandia and Indaianopolis and for the high grade metamorphosed rocks of the Barro Alto stratiform igneous complex, Goiàs State, Central Brasil. II° South Am Symp Isotopic Geology, Cordoba, Argentina, Actas, 31-33.

Correia, C.T., Girardi, V.A.V., Basei, M.A.S., Nutman, A., 2007. Cryogenian U–Pb (Shrimp I) zircon ages of anorthosites from the US of Niquelandia and Barro Alto Complexes, Central Brasil. Revista Brasileira de Geociências 37, 70-75.

Correia, C.T., Sinigoi, S., Girardi, V.A.V., Mazzucchelli, M., Tassinari, C.C.G., Giovanardi, T., 2012. The growth of large mafic intrusions: Comparing Niquelandia and Ivrea igneous complexes. Lithos 155, 167-182.

Della Giustina, M.E.S., Pimentel, M.M., Ferreira Filho, C.F., Fuck, R.A., Andrade, S., 2011. U–Pb–Hf-trace element systematics and geochronology of zircon from a granulite-facies metamorphosed mafic–ultramafic layered complex in Central Brazil. Precambrian Research 189, 172-192.

Ferreira Filho, C.F., Kamo, S., Fuck, R.A., Krogh, T.E., Naldret, A.J., 1994. Zircon and rutile geochronology of the Niquelândia layered mafic and ultramafic intrusion, Brazil: constraints for the timing of magmatism and high grade metamorphism. Precambrian Research 68, 241–255.

Ferreira Filho, C.F., Naldrett, A.J., Gorton, M.P., 1998. REE and pyroxene compositional variation across the Niquelândia layered intrusion, Brazil: petrological and metallogenetic implications. Transactions of the Institution of Mining and Metallurgy 107, B1-B21.

Ferreira Filho, C.S., Pimentel, M.M., Maria de Araujo, S., Laux, J.H., 2010. Layered intrusions and volcanic sequences in Central Brazil: geological and geochronological constraints for Mesoproterozoic (1.25 Ga) and Neoproterozoic (0.79 Ga) igneous associations. Precambrian Research 183, 617-634.

Fuck, R.A., Pimentel, M.M., Silva, L.J.H.D., 1994. Compartimentação tectônica da porção oriental da Província Tocantins. In: 38th Cong. Bras. Geologia, vol. 1 , 215–216.

Giovanardi, T., Lugli, F., 2017. The Hf-INATOR: A free data reduction spreadsheet for Lu/Hf isotope analysis. Earth Science Informatics, DOI 10.1007/s12145-017-0303-9.

Giovanardi, T., Girardi, V.A.V., Correia, C.T., Sinigoi, S., Tassinari, C.C.G., Mazzucchelli, M., 2015. U-Pb zircons SHRIMP data from the Cana Brava Layered Complex: New constraints for the mafic-ultramafic intrusions of Northern Goiás, Brazil. Open Geosciences7, 197-206.

Giovanardi, T., Girardi, V.A.V., Correia, C.T., Sinigoi, S., Tassinari, C.C.G., Mazzucchelli, M., 2017a. The growth and contamination mechanism of the Cana Brava layered mafic-ultramafic complex: new field and geochemical evidences. Mineralogy and Petrology 111, 291-314.

Giovanardi, T., Girardi, V.A.V., Correia, C.T., Tassinari, C.C.G., Sato, K., Cirpiani, A., Mazzucchelli, M., 2017b. New U–Pb SHRIMP-II zircon intrusion ages of the Cana Brava and Barro Alto layered complexes, central Brazil: Constraints on the genesis and evolution of the Tonian Goias Stratiform Complex. Lithos 282-283, 339-357.

Girardi, V.A.V., Kurat, G., 1982. Precambrian mafic and ultramafic rocks of the Cana Brava Complex, Brazil - mineral compositions and evolution. Revista Brasileira de Geociências 12(1-3), 313-323.

Girardi, V.A.V., Rivalenti, G., Sinigoi, S., 1981. Precambrian Barro Alto complex of Goias, Brazil: bulk geochemistry and phase equilibria. Neues Jahrbuch für Mineralogie Abhandlungen 142(3), 270-291.

Girardi, V.A.V., Rivalenti, G., Sinigoi, S., 1986. The petrogenesis of Niquelandia layered basic–ultrabasic complex, central Goias, Brasil. Journal of Petrology 27, 715-744.

Griffin, W.L., Pearson, N.J., Belousova, E., Jackson, S.E., van Achterbergh, E., O'Reilly, S.Y., Shee, S.R., 2000. The Hf isotope composition of cratonic mantle: LAM-MC-ICPMS analysis of zircon megacrysts in kimberlites. Geochimica et Cosmochimica Acta 64, 133–147.

Griffin, W.L., Wang, X., Jackson, S.E., Pearson, N.J., O'Reilly, S.Y., Xu, X., Zhou, X., 2002. Zircon chemistry and magma mixing, SE China: in-situ analysis of Hf isotopes, Tonglu and Pingtan igeous complexes. Lithos 61, 237-269.

Hawkesworth, C.J., Kemp, A.I.S., 2006. Using hafnium and oxygen isotopes in zircon to unravel the record of crustal evolution. Chemical Geology 226, 144–162.

Hoskin, P.O., Schaltegger, U., 2003. The composition of zircon and igneous and metamorphic petrogenesis. In Hanchar, J.M., Hoskin, P.O., eds, Zircon: Mineralogical Society of America Reviews in Mineralogy and Geochemistry 53, 27-62.

Kemp, A.I.S., Hawkesworth, C.J., Paterson, B.A., Kinny, P.D., 2006. Episodic growth of the gondwana supercontinent from hafnium and oxygen isotopes in zircon. Nature 439, 580–583.

Kinny, P.D., Maas, R., 2003. Lu–Hf and Sm–Nd isotope systems in zircon. In: Zircons, American Mineralogist, 327-341.

Ludwig, K.R., 2009. Isoplot 4.1. A geochronological toolkit for Microsoft Excel. Berkeley Geochronology Center special publication 4, 76.

Lugli, F., Brunelli, D., Cipriani, A., Bosi, G., Traversari, M., Gruppioni, G., 2017a. C4-Plant Foraging in Northern Italy: Stable Isotopes, Sr/Ca and Ba/Ca Data of Human Osteological Samples from Roccapelago (16th–18th Centuries AD). Archaeometry. doi: 10.1111/arcm.12295.

Lugli, F., Cipriani, A., Peretto, C., Mazzucchelli, M., Brunelli, D., 2017b. In situ high spatial resolution 87Sr/86Sr ratio determination of two Middle Pleistocene (c.a. 580 ka) *Stephanorhinus hundsheimensis* teeth by LA–MC–ICP–MS. International Journal of Mass Spectrometry 412, 38-48.

Moraes, R., Fuck, R.A., 1994. Deformação e metamorfismo das sequências Juscelândia e Serra da Malacacheta, Complexo Barro Alto, Goiás. Revista Brasileira de Geociências 24, 189–197.

Moraes, R., Fuck, R.A., 1999. Trajetória P–T Horária para oMetamorfismo da Sequência Juscelândia, Goiás: Condições do Metamorfismo e Implicações Tectônicas. Revista Brasileira de Geociências 29, 603–612.

Moraes, R., Fuck, R.A., Pimentel, M.M., Gioia, S.M.C.L., Figueiredo, A.M.G., 2003. Geochemistry and Sm–Nd isotope characteristics of bimodal volcanic rocks of Juscelândia, Goiás, Brazil: Mesoproterozoic transition from continental rift to ocean basin. Precambrian Research 125, 317-336.

Moraes, R., Fuck, R.A., Pimentel, M.M., Gioia, S.M.C.L., Hollanda, M.H.B.M., Armstrong, R., 2006. The bimodal rift-related volcanosedimentary sequence in Central Brazil: Mesoproterozoic extension and Neoproterozoic metamorphism. Journal of South American Earth Sciences 20, 287-301.

Nowell, G.M., Kempton, P.D., Noble, S.R., Fitton, J.G., Saunders, A.D., Mahoney, J.J., Taylor, R.N., 1998. High precision Hf isotope measurements of MORB and OIB by thermal ionisation mass spectrometry: insights into the depleted mantle. Chemical Geology 149, 211–233.

Pimentel, M.M., Fuck, R.A., 1992. Neoproterozoic crustal accrction in central Brazil. Geology 20, 375-379.

Oliveira Cordeiro, P.F., Oliveira, C.G., 2017. The Goiás Massif: Implications for a pre-Columbia 2.2–2.0 Ga continent-wide amalgamation cycle in central Brazil. Precambrian Research, 298, 403-420.

Pimentel, M.M., Fuck, R.A., Jost, H., Ferreira Filho, C.F., Araujo, S.M., 2000. The basement of the Brasília Fold Belt and the Goiás Magmatic Arc. In: Cordani UG, Milani EJ, Thomaz Filho A, Campos DA (Eds.), The Tectonic Evolution of South America, Rio de Janeiro. Proceedings of the 31st International Geological Congress, Rio de Janeiro, 195-229.

Pimentel, M.M., Ferreira Filho, C.F., Amstrong, R.A., 2004. Shrimp U–Pb and Sm–Nd ages of the Niquelandia Layered Complex: Meso (1,25 Ga) and Neoproterozoic (0,79 Ga) extensional events in Central Brasil. Precambrian Research 132, 132-135.

Pimentel, M.M., Ferreira Filho, C.F., Armele, A., 2006. Neoproterozoic age of the Niquelândia complex, Central Brazil: further ID-TIMS and Sm–Nd isotopic evidence. Journal of South American Earth Sciences 21, 228-238.

Rivalenti, G., Correia, C.T., Girardi, V.A.V., Mazzuchelli, M., Tassinari, C.C., Bertotto, G.W., 2008. Sr–Nd isotopic evidence for crustal contamination in the Niquelandia complex, Goiàs, Central Brasil. Journal of South American Earth Sciences 25, 298-312.

Sforna, M.C., Lugli, F., 2017. MapIT!: a simple and user-friendly MATLAB script to elaborate elemental distribution images from LA-ICP-MS data. Journal of Analytical Atomic Spectrometry 32, 1035-1043.

Stracke, A., Bizimis, M., Salters, V.J.M., 2003. Recycling oceanic crust: Quantitative constraints, Geochemistry Geophysics Geosystem 4(3), 8003, doi:10.1029/2001GC000223.

Trail, D., Watson, E.B., Tailby, N.D., 2012. Ce and Eu anomalies in zircon as proxies for the oxidation state of magmas. Geochimica et Cosmochimica Acta, 97, 70-87.

Vervoot, J.D., Kempt, A.I.S., 2016. Clarifyng the zircon Hf isotope record of crust-mantle evolution. Chemical Geology, 425, 65-75.

Williams, I.S., 1998. U-Th-Pb geochronology by ion microprobe. In: McKibben, M.A., Shanks, W.C.P., Ridley, W.I. (Eds.), Applications of Microanalytical Techniques to Understanding Mineralizing Processes, Reviews in Economic Geology 7, 1-35.

Yang, W.-B., Niu, H.-C., Shan, Q., Sun, W.-D., Zhang, H., Li, N.-B., Jiang, Y.-H., Yu, X.-Y., 2014. Geochemistry of magmatic and hydrothermal zircon from the highly evolved Baerzhe alkaline granite: implications for Zr–REE–Nb mineralization. Mineralium Deposita 49, 451-470.

Figure captions

Fig. 1: regional geotectonic setting of the Brasilia Belt modified after Oliveira Cordeiro and Oliveira (2017).

Fig. 2: geological map of the Cana Brava Complex, modified after Correia et al. (1997) and Giovanardi et al. (2017b).

Fig. 3: geological map of the Niquelândia Complex, modified after Correia et al. (2012) and Giovanardi et al. (2017b).

Fig. 4: geological map of the Barro Alto Complex, modified after Ferreira Filho et al. (2010) and Giovanardi et al. (2017b).

Fig. 5: $^{87}Sr/^{86}Sr$ and εNd recalculated at 790 Ma along the stratigraphy of the TGSC. Literature data from Niquelandia and Cana Brava are from Correia et al. (1997, 2012) and Giovanardi et al. (2017a).

Fig. 6: CL images of zircon grains from UGAZ Barro Alto anorthosite sample BA1541 reported with the number of the SHRIMP single spot analysis; calculated concordia and average $^{206}Pb/^{238}U$ age (errors are calculated as 2σ).

Fig. 7: CL images of zircon grains from MZ Niquelandia gabbro sample NQ15-49 reported with the number of the SHRIMP single spot analysis; calculated concordia and average $^{206}Pb/^{238}U$ age (errors are calculated as 2σ).

Fig. 8: CL images of zircon grains from UGAZ Niquelandia anorthosite sample NQ15-52 reported with the number of the SHRIMP single spot analysis; calculated concordia and average $^{206}Pb/^{238}U$ age (errors are calculated as 2σ).

Fig. 9: recalculated εHf(t) for zircon grains with measured U-Pb ages. (1) literature data from Della Giustina et al. (2011). The depleted mantle (DM) evolution line is calculated using the values of present-day $^{176}Hf/^{177}Hf$ ratio of 0.28325 from Nowell et al. (1998) and $^{176}Lu/^{177}Hf$ ratio of 0.0384 from Griffin et al. (2000). CHUR values are from Blichert-Toft and Albarede (1997).

Fig. 10: zircons REE patterns normalized to the Chondrite I composition (CI; Anders and Edibara 1992). In each panel, the minimum and maximum $^{206}Pb/^{238}U$ ages in Ma otained with LA-ICP-MS are reported.

Fig. 11: recalculated εHf(t) for zircon grains with measured U-Pb ages. (1) literature data from Della Giustina et al. (2011). The depleted mantle (DM) evolution line is calculated using the values of present-day $^{176}Hf/^{177}Hf$ ratio of 0.28325 from Nowell et al. (1998) and $^{176}Lu/^{177}Hf$ ratio of 0.0384 from Griffin et al. (2000). CHUR values are from Blichert-Toft and Albarede (1997). US and LS inherited fields are the recalculated εHf of inherited zircons at 1.3Ga. US and LS inherited avg are

the evolutions through time of εHf from average inherited zircons. US and LS crust are the extimated evolutions through time of εHf from inherited bulk rock calculated from average $^{176}Hf/^{177}Hf$ initial ratio from inherited zircons and $^{176}Lu/^{177}Hf$ ratio of 0.015 for the continental crust bulk rock from Griffin et al. (2002), the average of MORB at 0.024 (Stracke et al., 2003) and minimum, maximum and average ratios of bulk-rock analysis of xenoliths from LS (Correia et al., 2012) and amphibolites (Moraes et al., 2003).

Table captions

Table 1: sample coordinates and references for previously published U-Pb data.

Table 2: average of Lu-Hf isotopic data from magmatic and inherited zircons. εHf, $\varepsilon Hf_{(t)}$, T_{DM} and T_{DM}^{C} are calculated using the Hf-INATOR spreadsheet (Giovanardi and Lugli, 2017). T_{DM} and T_{DM}^{C} are in Ma. M are magmatic zircons whose ages are consistent with the TGSC intrusion age; I are inherited zircons.

Table 3: solution and in situ Sr isotope ratios from plagioclases from Barro Alto.

Figure 1

Click here to download high resolution image

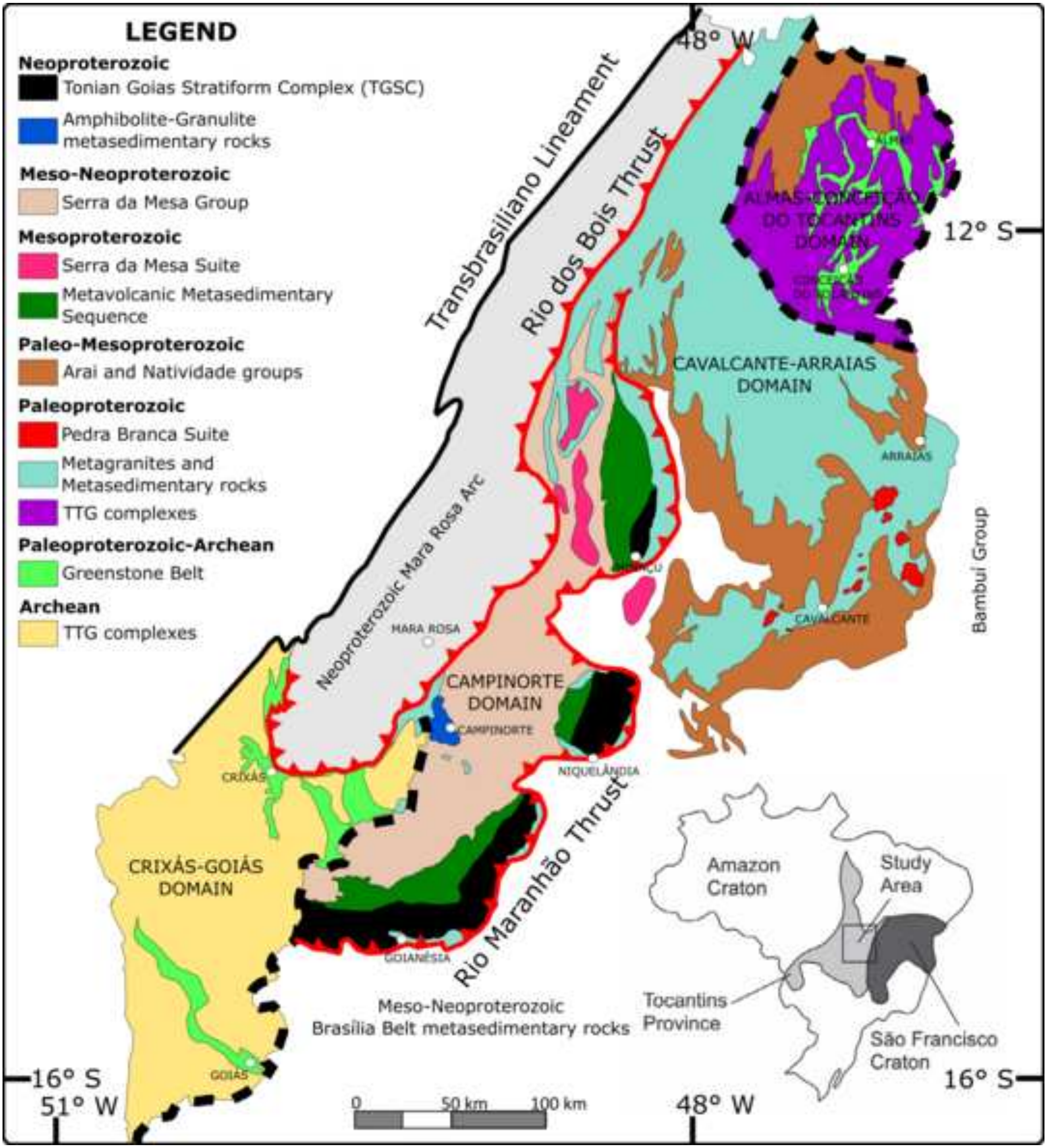

Figure 2
Click here to download high resolution image

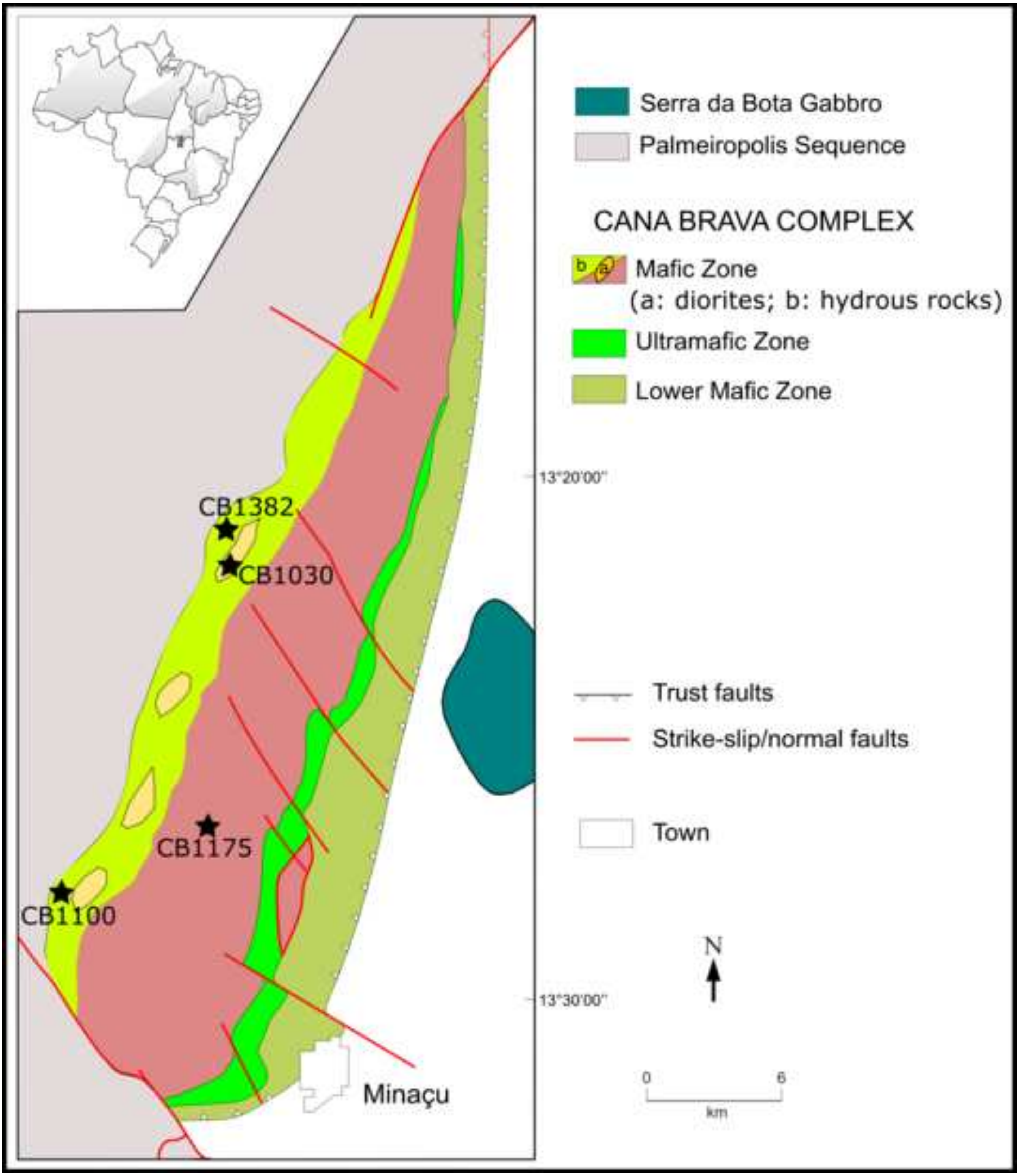

Figure 3

Click here to download high resolution image

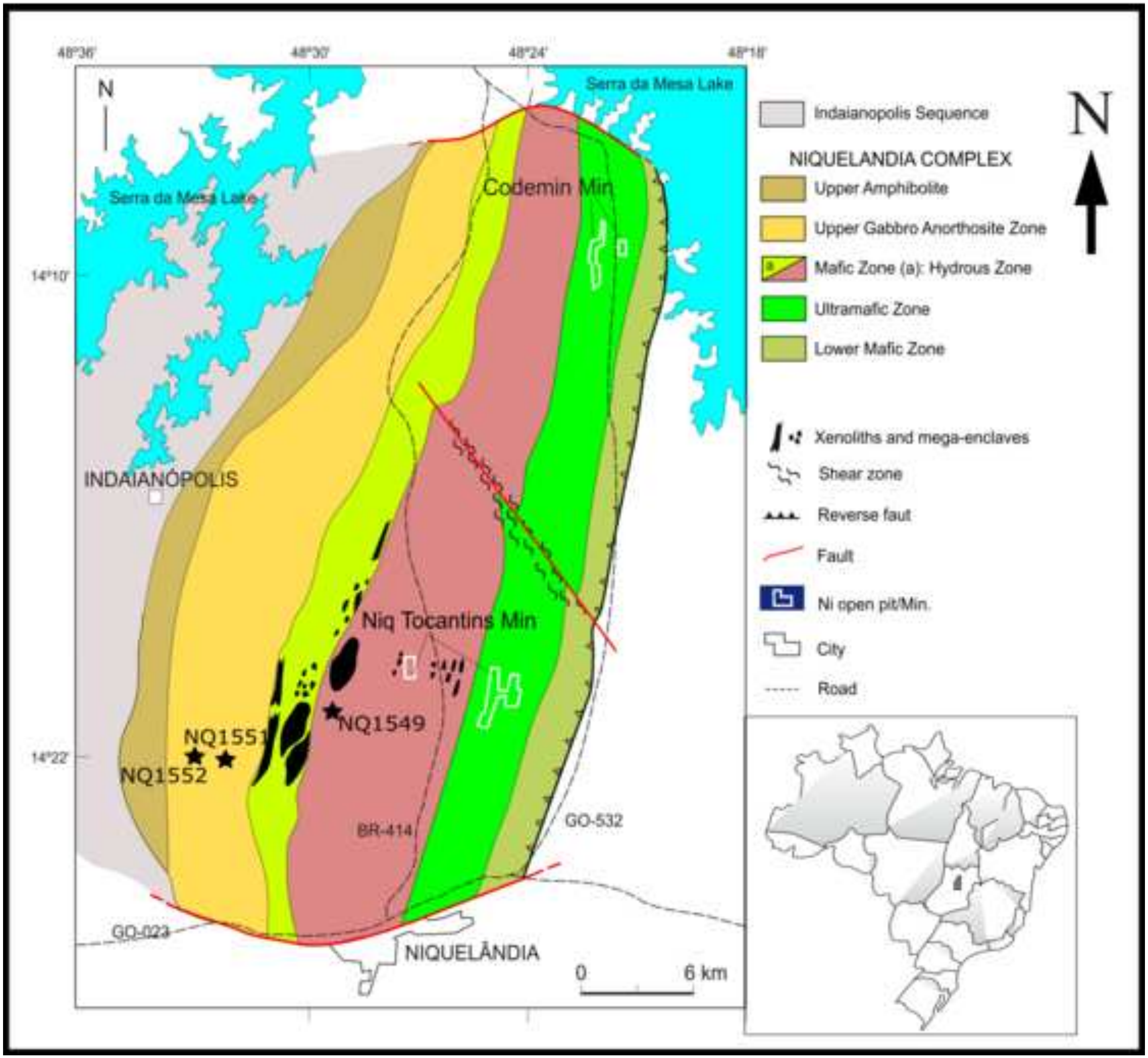

Figure 4
Click here to download high resolution image

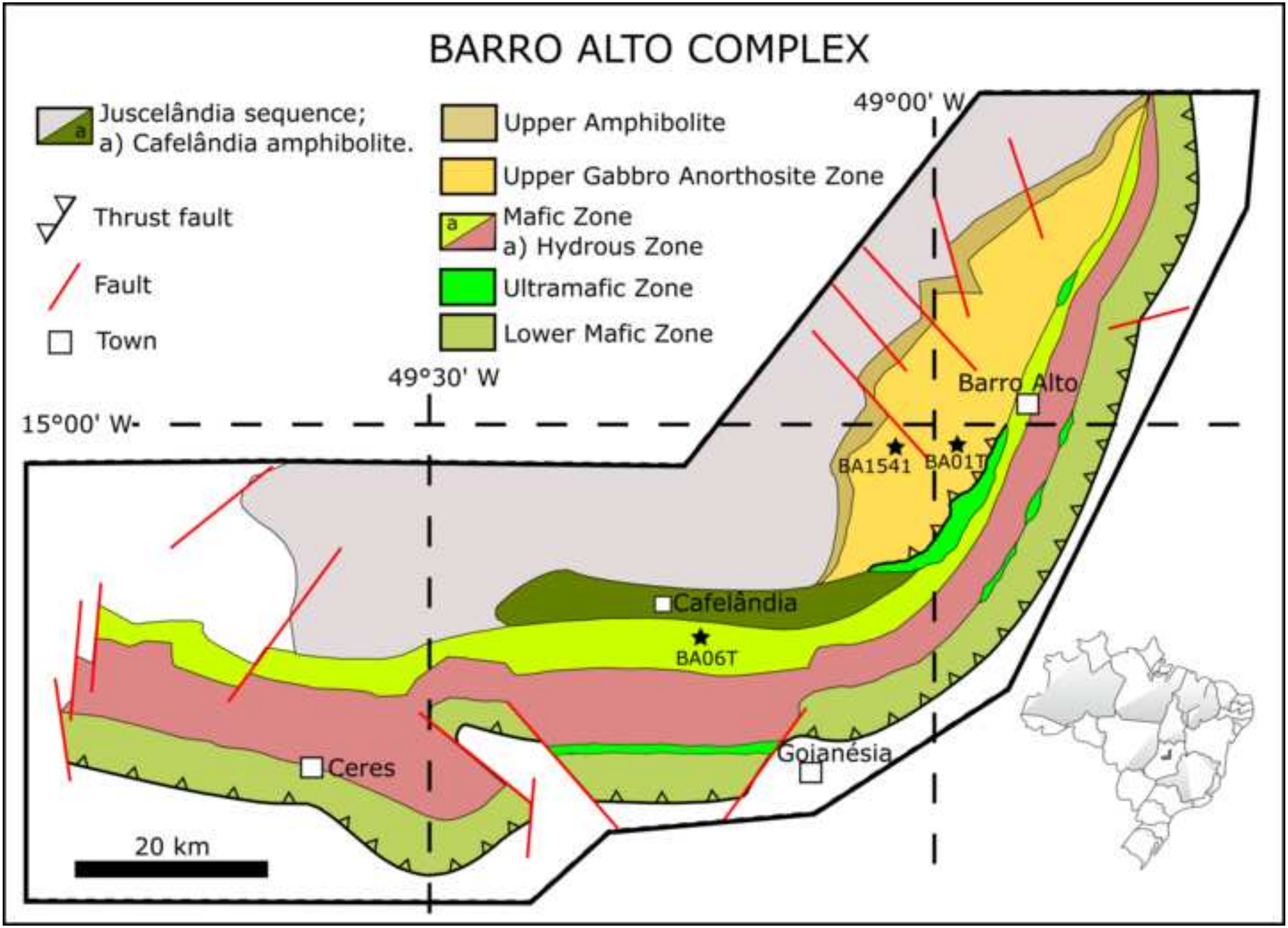

Figure 5
Click here to download high resolution image

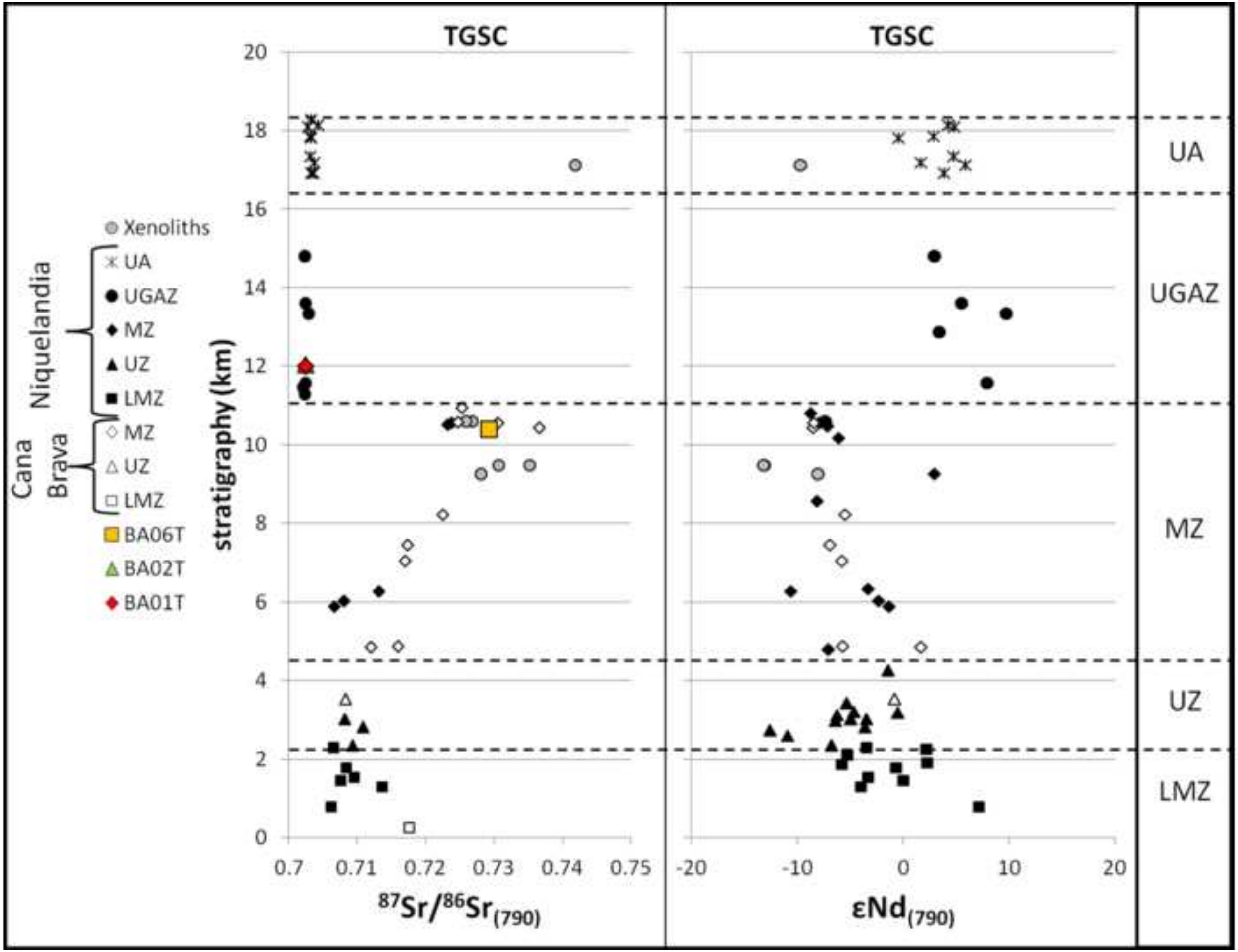

Figure 6
Click here to download high resolution image

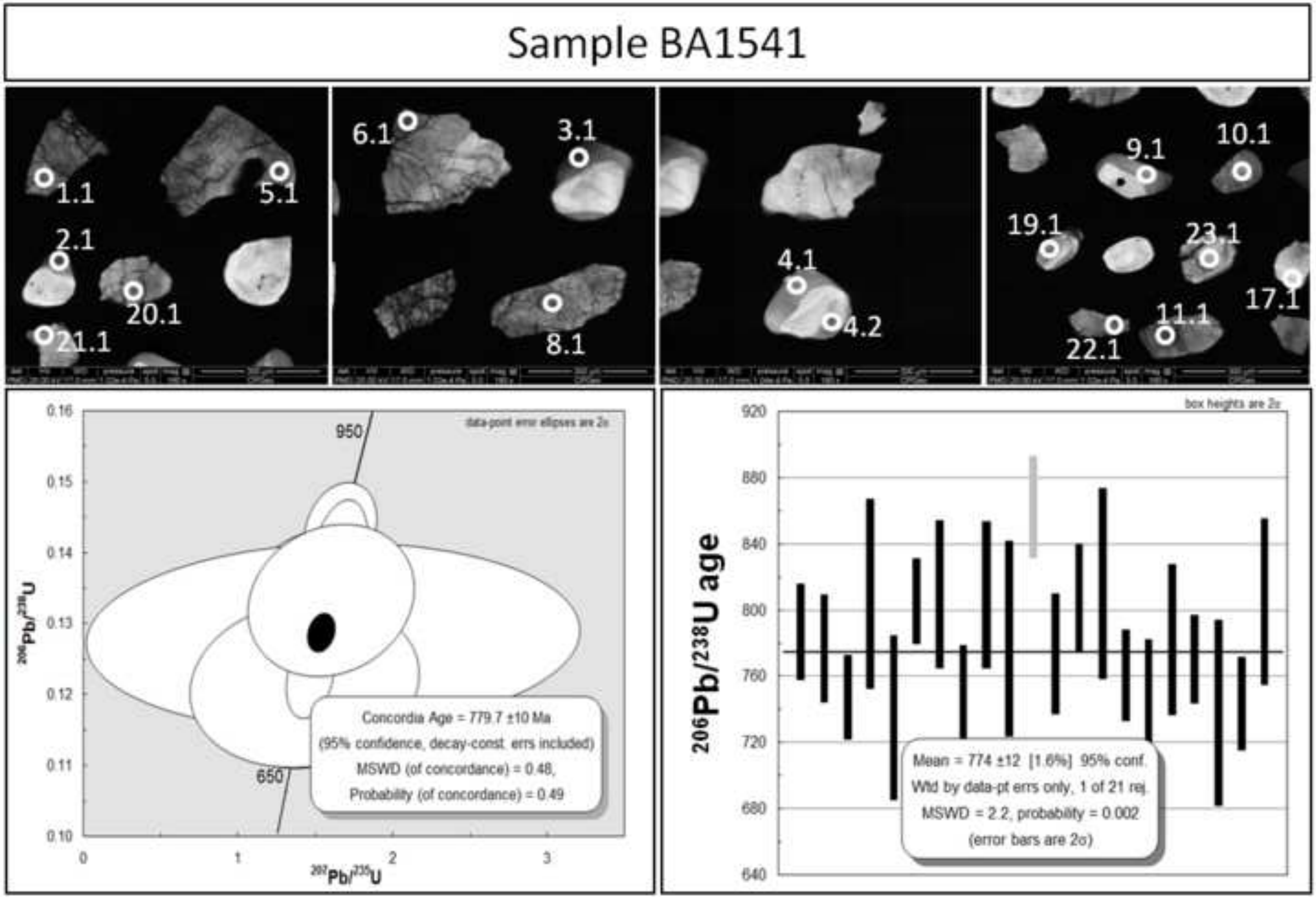

Figure 7

Click here to download high resolution image

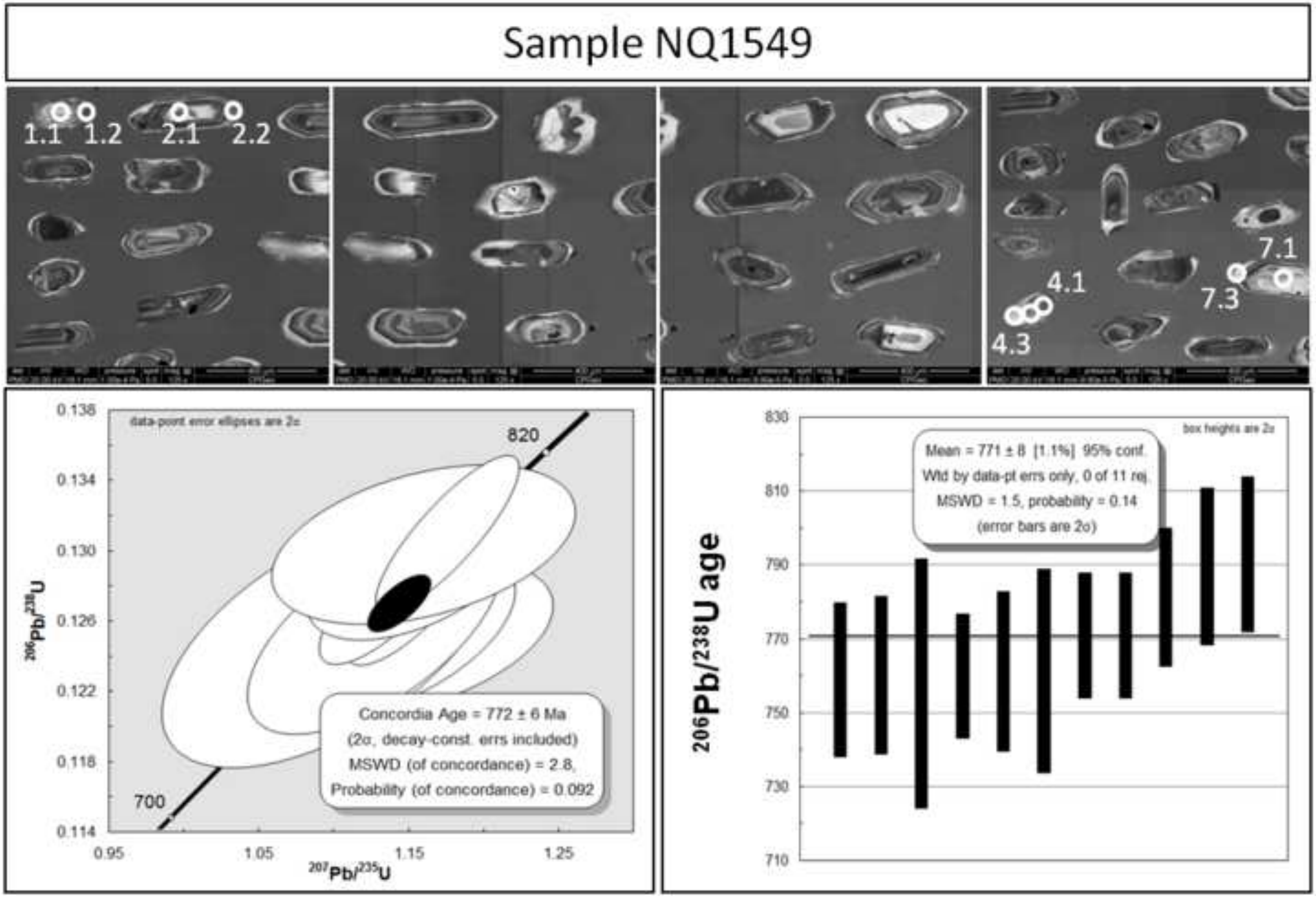

Figure 8
Click here to download high resolution image

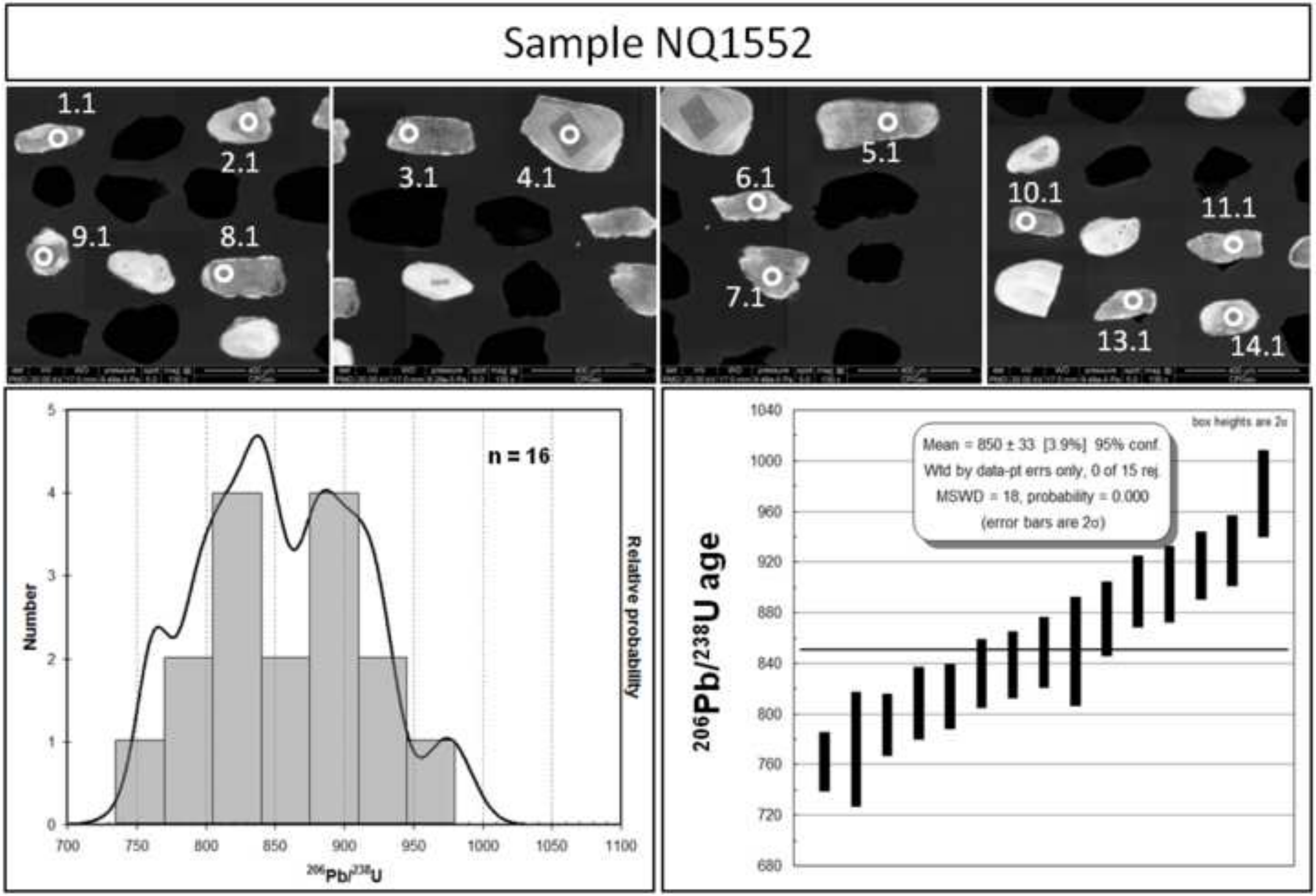

Figure 9
Click here to download high resolution image

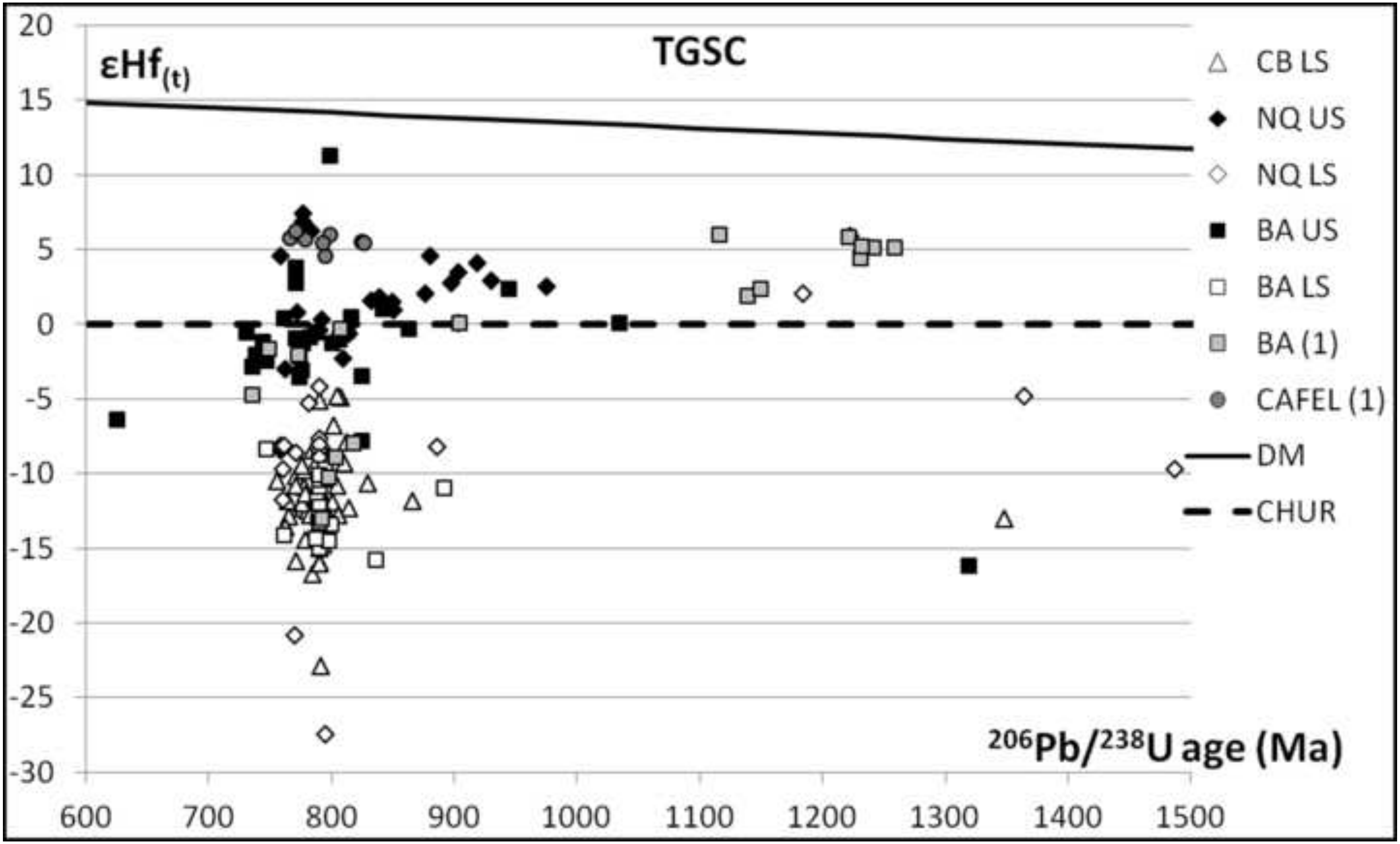

Figure 10
Click here to download high resolution image

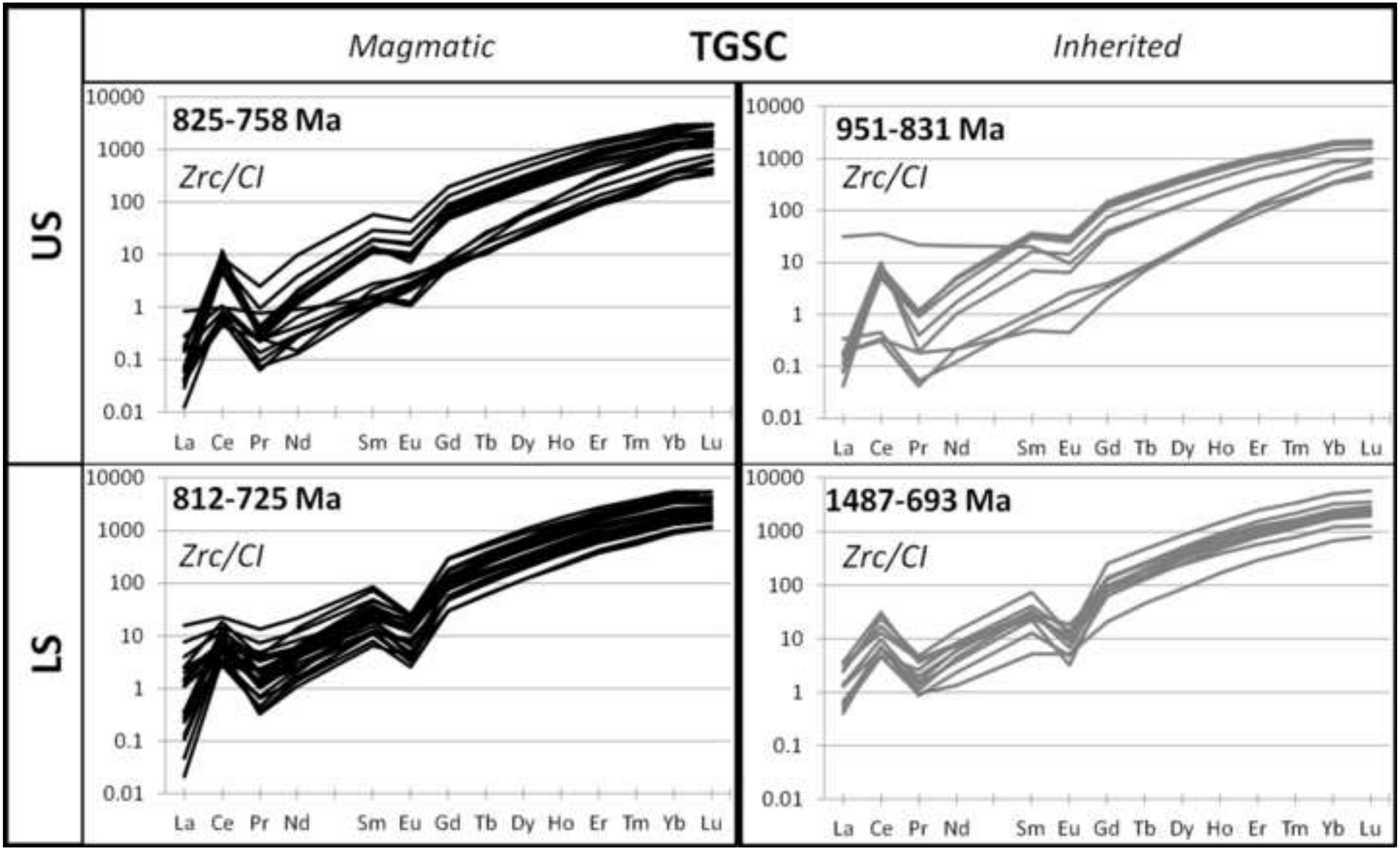

Figure 11
Click here to download high resolution image

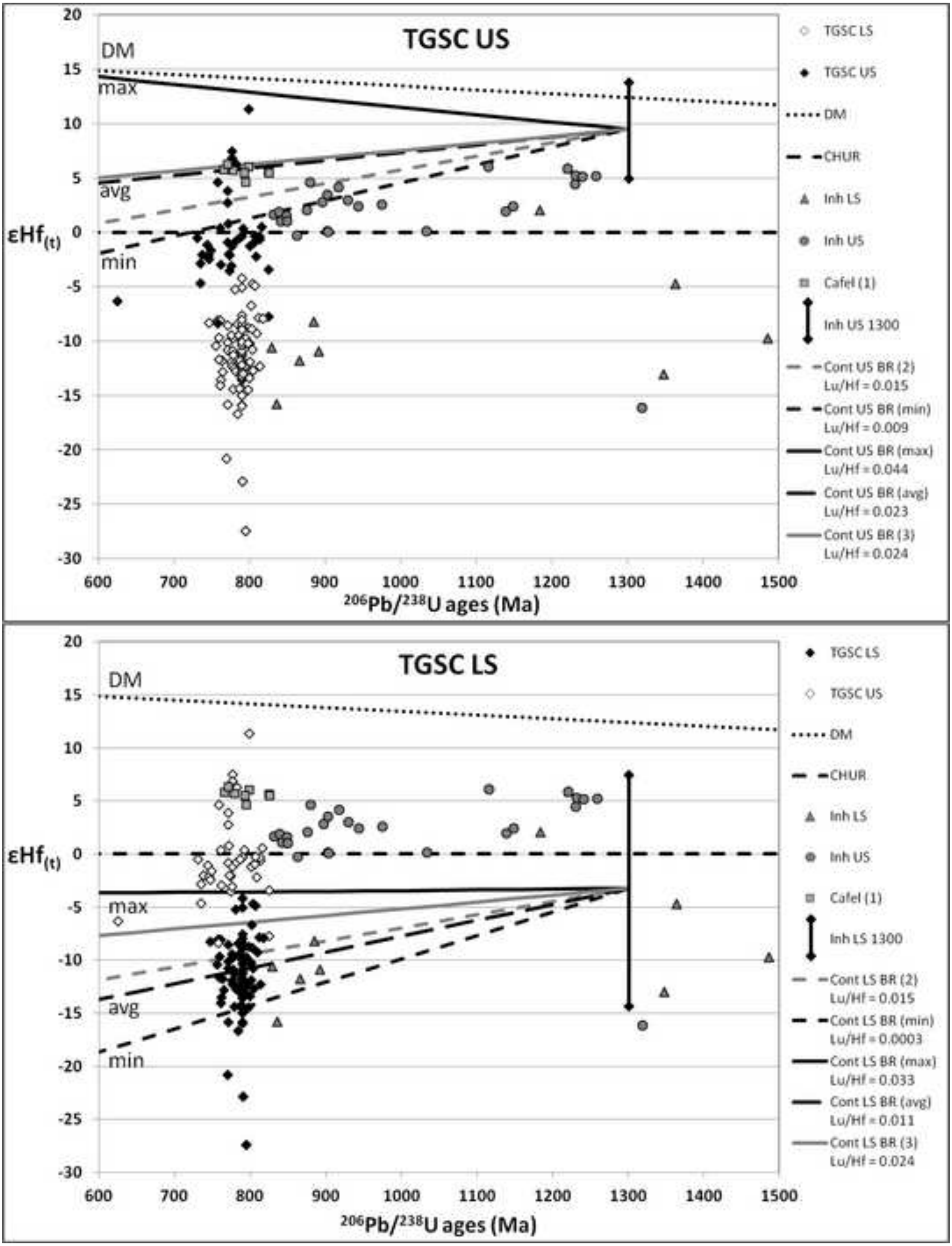

Table 1

Click here to download Table: Table 1.docx

Sample	Complex	Sequence	Longitude	Latitude	Lithology	Reference
CB1030	Cana Brava	LS	48°15'21.99"W	13°22'9.49"S	Diorite	Giovanardi et al. 2015, 2017b
CB1100	Cana Brava	LS	48°18'38.12"W	13°29'10.48"S	Gabbro	Giovanardi et al. 2015, 2017b
CB1175	Cana Brava	LS	48°16'3.61"W	13°28'0.01"S	Gabbro	Giovanardi et al. 2015, 2017b
CB1382	Cana Brava	LS	48°15'32.05"W	13°22'6.06"S	Gabbro	Giovanardi et al. 2015, 2017b
NQ1549	Niquelandia	LS	48°29'56.40"W	14°21'49.59"S	Gabbro	This work
NQ1551	Niquelandia	US	48°31′39.40″W	14°22′4.59″S	Anorthosite	Correia et al. 2012
NQ1552	Niquelandia	US	48°31’58”W	14°22’01”S	Anorthosite	Correia et al. 2007
BA06T	Barro Alto	LS	49°11'23.94"W	15°12'51.04"S	Gabbro	Giovanardi et al. 2017b
BA01T	Barro Alto	US	48°59'17.91"W	15°05'02.13"S	Anorthosite	Giovanardi et al. 2017b
BA1541	Barro Alto	US	49°02’25”W	15°05’17”S	Anorthosite	Correia et al. 2007

Table 2

Click here to download Table: Table 2.docx

Sample	Complex	Sequence		$^{176}Yb/^{177}Hf$	2σ	$^{176}Lu/^{177}Hf$	2σ	$^{176}Hf/^{177}Hf$	2σ	$^{178}Hf/^{177}Hf$	2σ	avg. ^{180}Hf	$eHf_{(0)}$	$eHf_{(t)}$	T_{DM}	T_{DM}^{C}
CB1030	CB	LS	M	0.042613	0.019526	0.000899	0.000313	0.281977	0.000111	1.467317	0.000121	1.34	-28.1	-11.4	1788	2427
CB1175	CB	LS	M	0.039609	0.048404	0.000861	0.000984	0.281995	0.000248	1.467319	0.000042	1.75	-27.5	-10.2	1761	2369
CB1382	CB	LS	M	0.074620	0.049375	0.001702	0.001208	0.281989	0.000107	1.467226	0.000097	2.29	-27.7	-11.3	1811	2459
CB1100	CB	LS	M	0.045385	0.023267	0.001043	0.000558	0.281903	0.000087	1.467259	0.000084	1.58	-30.7	-14.0	1898	2602
CB1100	CB	LS	I	0.052625	0.009577	0.001186	0.000207	0.281826	0.000414	1.467210	0.000042	1.61	-33.4	-11.8	2011	2641
NQ1549	NQ	LS	M	0.041487	0.030286	0.000970	0.000705	0.282002	0.000345	1.467325	0.000045	1.58	-27.3	-10.6	1756	2375
NQ1549	NQ	LS	I	0.044257	0.031025	0.001043	0.000723	0.281943	0.000475	1.467307	0.000034	1.53	-29.3	-3.0	1843	2233
NQ1552	NQ	US	M	0.032539	0.020619	0.000780	0.000381	0.282266	0.000088	1.467324	0.000121	1.04	-17.9	-0.9	1382	1758
NQ1552	NQ	US	I	0.037825	0.020249	0.000879	0.000423	0.282300	0.000071	1.467323	0.000085	1.00	-16.7	2.4	1340	1626
NQ1551	NQ	US	M	0.016588	0.012707	0.000466	0.000311	0.282392	0.000364	1.467318	0.000234	0.90	-13.4	3.4	1197	1467
BA06T	BA	LS	M	0.039564	0.033874	0.000901	0.000720	0.281945	0.000110	1.467307	0.000114	1.27	-29.3	-12.4	1833	2495
BA06T	BA	LS	I	0.036741	0.046638	0.000912	0.000913	0.281870	0.000131	1.467257	0.000015	1.39	-31.9	-13.4	1937	2616
BA01T	BA	US	M	0.019470	0.038147	0.000523	0.001017	0.282289	0.000306	1.467294	0.000074	1.74	-17.1	0.3	1343	1688
BA01T	BA	US	I	0.050026	0.015659	0.001247	0.000341	0.281908	0.001088	1.467327	0.000010	1.95	-30.6	-7.6	1900	2418
BA1541	BA	US	M	0.024335	0.032836	0.000595	0.000708	0.282262	0.000066	1.467317	0.000083	1.69	-18.0	-1.4	1382	1771
BA1541	BA	US	I	0.035952	0.051749	0.000879	0.001222	0.282217	0.000109	1.467306	0.000205	1.63	-19.6	0.8	1456	1778

Table 3
Click here to download Table: Table 3.docx

Sample	**Unit**	**$^{87}Sr/^{86}Sr$**	**2σ**	**Rb/Sr**	**$^{87}Sr/^{86}Sr_{(790)}$**
solution					
BA02T	UGAZ	0.702368	0.000012	0.0020	0.702355
BA06T	MZ	0.729226	0.000012	0.0030	0.729192
in situ					
BA01T	UGAZ	0.702452	0.000040	0.0011	0.702430
BA02T	UGAZ	0.702444	0.000329	0.0020	0.702432
BA06T	MZ	0.729948	0.000125	0.0030	0.729914

Supplementary Material Table A

Click here to download Background dataset for online publication only: Supplementary Material A_U-Pb.xlsx

Supplementary Material Table B

Click here to download Background dataset for online publication only: Supplementary Material B_Lu Hf.xlsx

Supplementary Material Table C

Click here to download Background dataset for online publication only: Supplementary Material C_trace.xlsx